N72-18429

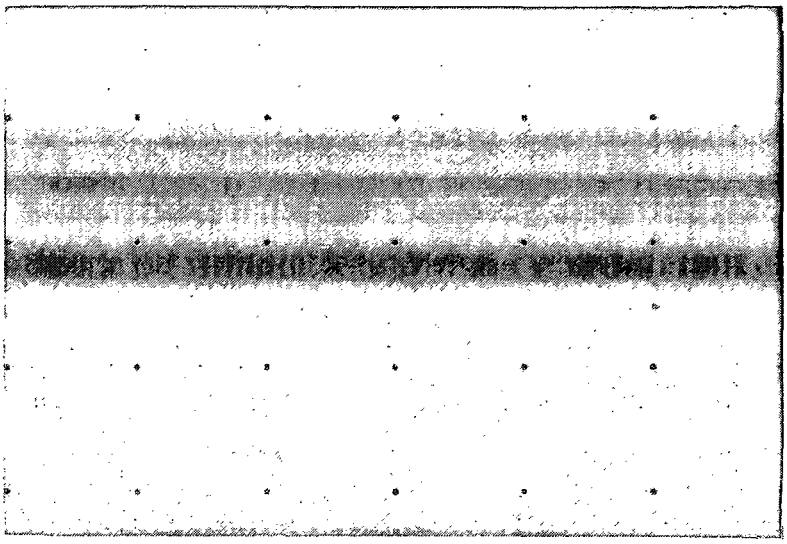

NRC NATIONAL RESEARCH CORPORATION
A SUBSIDIARY OF CABOT CORPORATION
CAMBRIDGE, MASSACHUSETTS 02142

NASA CR-111986

WIND TUNNEL MASS SPECTROMETER DESIGN STUDY

J. E. Hueser
P. Fowler

FINAL REPORT

Prepared Under Contract No.
NAS1-8223-6

NATIONAL RESEARCH CORPORATION
(A Subsidiary of Cabot Corporation)
70 Memorial Drive
Cambridge, Massachusetts 02142

for

NATIONAL AERONAUTICS AND SPACE ADMINISTRATION

TABLE OF CONTENTS

LIST OF FIGURES

LIST OF TABLES

WIND TUNNEL MASS SPECTROMETER DESIGN STUDY

By J. E. Hueser and P. Fowler
National Research Corporation
(A Subsidiary of Cabot Corporation)

SUMMARY

This study evaluates the design parameters of a sampling probe which is to measure the free stream gas composition in a hypersonic wind tunnel. Using a free expansion of the hypersonic continuum tunnel flow, a series of sampling inlet-pumping stages are evaluated. Mass analysis is carried out with a quadrupole mass spectrometer employing a crossed electron beam, molecular beam ion source and an off-axis electron multiplier. The spatial distribution of the sampled molecular flux and the pumping requirements are evaluated for varying inlet conditions of gas density and flow velocity. The signal-to-noise ratio of the molecular beam formed by this series of coaxial inlets is also determined. It is concluded that the signal-to-noise ratio of the unscattered flux is sufficiently high ($\approx$ 50) that an unambiguous determination of the beam composition and therefore, of the free stream gas properties can be made. The magnitude of the detected signal is sufficiently high that measurement of trace constituents two orders of magnitude below the primary beam signal can be made.

The pumping requirements and the performance characteristics of titanium sublimation sources, using 77°K condensing surfaces, are evaluated for use with the sampling probe. For

an assumed capture coefficient of 0.4 for hydrogen on titanium, sublimation pumps can handle the gas load in the expansion chambers of the compound (at least four stages) inlet system except for Mach numbers greater than $\approx$ 10. The possibility and advantages of using compound pumping systems consisting of LHe cryopumping and cryogettering, considering a cryosubstrate temperature of 20°K, are also discussed.

In conclusion, this analysis shows that the maximum inlet density to the free-molecular inlet stage of the sampling system is approximately 7.5×10^{15} cm^{-3} at a temperature of 120°K ($\approx$ 0.1 Torr). This upper limit is imposed by both the minimum dimensions of the inlet and the maximum pumping efficiency. The limitation in the total sampling system performance is determined by the pumping speed required in the continuum sampling stage.

1. INTRODUCTION

The purpose of this study is to investigate the design of an instrument to measure the density and composition in the free stream flow of a hypersonic wind tunnel. The diagnostic benefits of such a probe are twofold in that it allows an optimization of source nozzle parameters and permits a direct measurement of the free stream gas kinetic properties. The large static pressure and mass flow rate both exclude the possibility of using remote instrumentation tubulated into the tunnel. The approach required is to introduce the sampler

probe and associated detector directly into the tunnel in such a way that it perturbs the tunnel flow as little as possible so that direct correlation is maintained between the sampled gas flow and free stream gas flow. Shock formation must be avoided since it would obliterate the correlation between the sampled and free stream composition due to dissociation or synthesis of molecules. The approach to the problem is to choose the appropriate inlet and pumping stages to reduce the hypersonic continuum flow, by means of a series of expansion chambers, to supersonic free molecular flow for subsequent mass spectrometer analysis of the component gases. The general requirement of each successive inlet stage is to choose the minimum geometrical dimensions consistent with the preservation of hypersonic or supersonic flow and provide for pumping the high molecular flux which is stripped from the total flow and results in a molecular beam formed by the series of coaxial inlets.

2. STATEMENT OF THE PROBLEM

The general requirement of the sampling system is to extract a specimen of the high pressure hypersonic tunnel flow and by pumping the expanded portion of the flow while admitting the central core of the flow into successive expansion chambers, inlet-pumping stages, to reduce the molecular density in the resulting molecular beam to a level which can be analyzed by means of a quadrupole mass spectrometer.

In order for the composition analysis derived from the mass spectrometer measurements to retain a correlation with the free stream composition, the pumping system in the expansion chambers must reduce the background density to a negligible level with respect to the molecular beam density. Since this signal-to-noise ratio is a function of the flow velocity, the analysis requires an evaluation of the sampled gas flux distribution to estimate both the beam density and the pumping efficiency of this non-equilibrium flow.

The requirement for high pumping capacity in a constrained geometry necessitates the maximum utilization of the available sampler probe wall surface area. Because of conductance limitations, attached or tubulated pumps such as ion or diffusion pumps cannot compete with surface pumping, either cryopumping or sorption pumping. Since hydrogen is one of the main constituents of the combustion chamber reactions, the cryosurface temperature of an anticipated cryopumped system must be maintained at the minimum practicable limit to keep the background hydrogen partial pressure at a reasonable level. Taking this limit to be 4.2°K, the temperature of free boiling liquid helium, the equilibrium hydrogen vapor pressure would be approximately 4×10^{-7} Torr, which is the same order of magnitude as the anticipated molecular beam density at the ion source. Since this would result in an unacceptable S/N ratio, additional methods of pumping the hydrogen must be evaluated, at least in the ion source chamber. Sorption pumping, specifically cryogenic titanium

sublimation pumping, may be used for the removal of hydrogen in the expansion stages of the compound inlet system. Pumping of other gases expected to be present, such as N_2, O_2, CO_2, CO, and H_2O is readily accomplished with this system although the use of the probe in tunnels with a large methane component may present difficulties due to the generally low capture coefficient for that gas. Cryogenic getter pumping is the primary pumping mechanism although the possibility of a compound system consisting of both cryopumping in the higher pressure stages together with cryogettering in the low pressure stage may be more satisfactory.

A schematic representation of the sampling probe is shown in Figure 1. The first stage inlet, a hypersonic continuum inlet, has not been specifically evaluated. It has however been assumed that the flow through this sampling stage (either a single or compound stage) remains hypersonic and that sufficient pumping is available to accomplish this. In analogy to a skimmer sampling of a free jet expansion, the next stage is a near free molecular sampling inlet. Although the two are analogous in concept, they are not the same since the free jet expansion is from a stagnation region while the first stage in this case is an expansion of a sampled hypersonic flow region. For this reason, neither the functional dependence of the flow velocity (Mach number) nor the free stream density with distance behind the inlet are known exactly. However, it is safe to assume that the free stream density is lower and the Mach number higher at the inlet to the following stage. From the near free molecular flow inlet

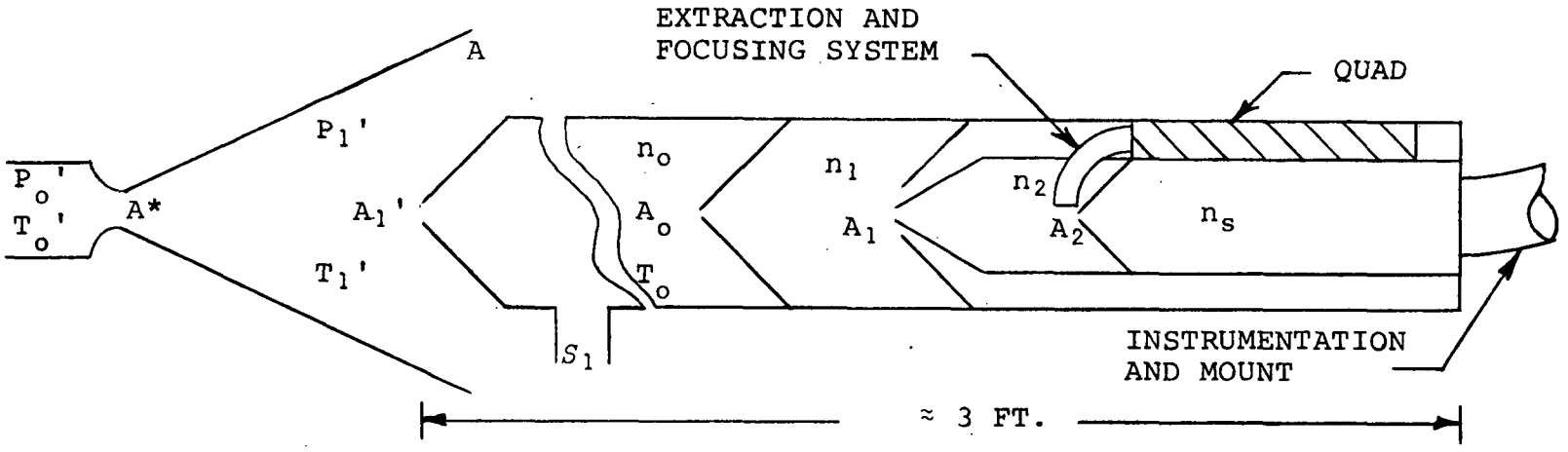

P_o',T_o' = Tunnel Stagnation Conditions
P_1',T_1' = Tunnel Static Conditions
A*, A = Nozzle Throat and Exit Areas
A_1' = Hypersonic Inlet Area
S_1 = Continuum Stage Pumping Speed
n_o = Free Molecular Inlet Density
A_o = Free Molecular Inlet Area
T_o = Gas Temperature at Free Molecular Inlet
n_1, A_1 = Inlet Conditions at the Mass Spectrometer Inlet
n_2 = Background Density at the Ion Source
A_2 = Inlet Area at the Probe Stagnation Stage
n_s = Probe Stagnation Density

Figure 1.
Schematic Representation of the Tunnel Sampling Probe

(the mean free path is equal to the inlet diameter), the flow parameters are analyzed in detail using a range of Mach numbers (6-15) and a maximum molecular density of 7.5×10^{15} cm^{-3}. From this parametric analysis, the maximum inlet density at a given Mach number which can be handled by the interstage pumping systems can be arrived at. These results when coupled with the analysis of the flow field behind the hypersonic inlet will permit an estimate of the maximum tunnel density which can be handled by the entire probe system.

3. GAS-SURFACE INTERACTION PARAMETERS

The evaluation of the sorption pumping mechanism requires that values be assigned to the physical parameters controlling the gas-surface interactions. In the case of an effusive gas stream entering the pumping region, these parameters have been experimentally determined for a variety of gas-surface combinations and the assumption of complete energy accommodation and a diffuse scattering distribution is generally valid. On the other hand, the understanding of the interaction of a supersonic beam with the pumping surface is incomplete and the justification for an assumed energy accommodation and scattered spatial distribution depends on the gas-surface pair to be considered and the interaction parameters involved. The choice of the hydrogen-titanium system is appropriate to this investigation since H_2 will

be one of the predominant gases in the tunnel flow and will also be one of the most difficult to pump. The results will therefore, reflect this worst case choice. Titanium is chosen as the sublimation material primarily because there is more data available for it than others. This does not rule out the use of other materials such as Mo or Ta.

A set of general gas surface interaction characteristics which apply to supersonic beams ($0 < E_i < 20$ eV) have been discussed by Stickney (ref. 1). These interaction characteristics, represented shcematically in Figure 2, help to specify the average energy and the spatial distribution of reflected molecules for a given set of boundary conditions and are as follows:

1. $\partial \phi_{r_{max}} / \partial T_g \geq 0$ if the molecular beam has a Maxwellian velocity distribution. (If the beam is monoenergetic, then the corresponding characteristic is $\partial \phi_{r_{max}} / \partial U_i \geq 0$ or $\partial \phi_{r_{max}} / \partial E_i \geq 0$).

2. $\partial \phi_{r_{max}} / \partial T_s \leq 0$ if the composition and structure of the target surface do not vary with T_s.

3. $\partial \phi_{r_{max}} / \partial \phi_i \geq 0$.

4. $\partial \phi_{r_{max}} / \partial m_g < 0$ when $\phi_{r_{max}} < \phi_i$ (i.e., subspecular scattering), whereas $\partial \phi_{r_{max}} / \partial m_g > 0$ when $\phi_{r_{max}} > \phi_i$ (i.e., supraspecular scattering).*

5. The dispersion or half-width of a scattering pattern increases with the energy of adsorption and/or with m_g, the molecular mass.*

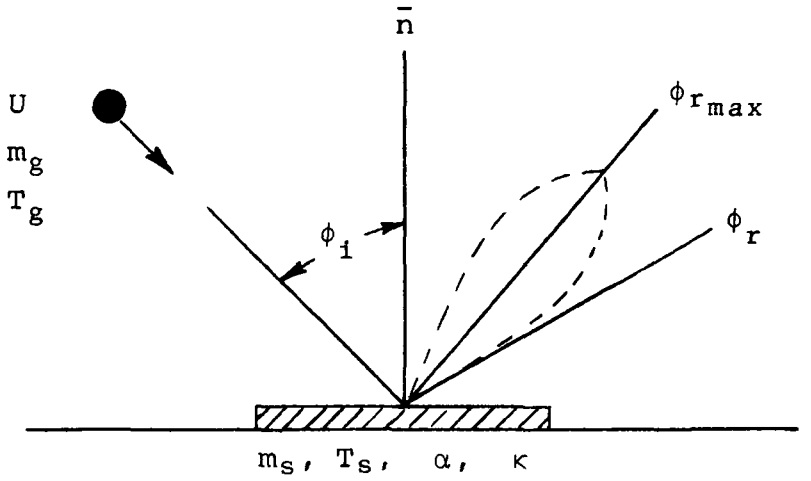

m_g = Gas Molecular Mass
m_s = Solid Surface Molecular Mass
T_g = Gas Temperature
T_s = Surface Temperature
U = Incident Gas Velocity
α = Energy Accommodation Coefficient
κ = Capture Coefficient
ϕ_i = Angle of Incidence
ϕ_r = Angle of Reflection
$\phi_{r_{max}}$ = Angle of Maximum Reflected Flux.

Figure 2
Representation of a Typical Gas-Surface Interaction

6. Supraspecular patterns (i.e., $\phi_{r_{max}} > \phi_i$) are most likely to occur when both of the following conditions are met: (a) $T_g > T_s$ and (b) $\phi_i << 90°$.

7. Nondiffuse or lobular scattering is most likely to occur from target surfaces that are both smooth and free of gross contamination.

8. The dispersion or half-width for nondiffuse scattering is greater for the in-plane pattern than for the out-of-plane pattern. (That is, the probability is low that molecules will be scattered out of the plane defined by the incident beam and the target normal).

In the computation of pumping performance, the following must be specified:

1. The energy and angular dependence of the accommodation (α) and capture (κ) coefficients

2. The dependence of α and κ on surface parameters such as temperature, gas coverage, homogeniety and roughness

3. The effect of surface parameters on deposition rate, diffusion rate, and pressure

Since the sorption process (pumping) is a combination of physisorption, chemisorption, and bulk diffusion, the problem of specifying the energy accommodation (potential scattering of an incoming gas molecule with the crystal lattice) or the capture coefficient (a combination of the adsorption-desorption

---

*Although it appears that the scattering pattern depends both on m_g and on the adsorption energy it is difficult to determine the effects of each individually because both change when we select a different beam gas. Hence, characteristics 4 and 5 are not as definite or as general as 1, 2 and 3.

processes) is difficult to accomplish theoretically and since the necessay experimental data is not available, certain of the parameters must be inferred from the effusive source data together with general characteristics of the supersonic beam data. The parameters which are left unspecified will be evaluated over a range of values of the other parameters and conclusions can be drawn concerning the validity of the results. For example, a parametric survey of the inlet conditions (density, speed ratio, and gas temperature) in terms of the required pressure drop from one inlet stage to the next will require a certain capture coefficient for the pumping surface. If the calculated value required for the necessary pressure drop is greater than the experimental value for an effusive source, then the inlet conditions are excessive. In this manner, a set of inlet conditions (within a range of uncertainty) which are maximized with respect to plausible values of unknown parameters can be established.

The general interaction characteristics discussed above together with the experimental data of Brown et al. (ref. 2) and Caldwell et al. (ref. 3) indicate, for the conditions to be met in this feasibility analysis, that the energy accommodation coefficient is nearly unity and therefore, the assumption will be made that the flux scattered from the titanium pumping surfaces is diffuse and distributed as a Maxwellian gas with a temperature characteristic of the sublimation pump substrate temperature. Additional support for this assumption is the

fact that titanium evaporated onto a 77°K surface has a poorly defined crystal structure indicating a rather rough surface. With substrate temperatures of 77°K there will also be formed cryodeposits of condensible gases such as H_2O and CO_2 which also produce a porous, rough surface. As discussed in refs. 1, 2 and 3, these effects tend to produce diffuse reflected flux distributions.

The data of Clausing (ref. 4), Moody (ref. 5), Elsworth, et al. (ref. 6) and Kindall (ref. 7), present the pertinent variables controlling the capture coefficient of H_2 on Ti. Although there are differences concerning the capture coefficient as related to various film preparation and measurement procedures, the data is consistent concerning the functional dependence of the capture coefficient with temperature and gas coverage. These data are presented in Table I and Figure 3. None of these data are molecular beam measurements, although Moody's data is a close approximation and is perhaps more reliable since he makes an attempt to measure the flux directly leaving the surfaces. It can also be concluded that during continuous evaporation hydrogen is removed from the gas phase on a one-to-one basis and therefore is probably chemisorbed as TiH_2, since the process is non-reversible upon warming up the substrate. However, there is some discrepency concerning the magnitude of the capture coefficient as a function of temperature. As can be seen from Table I, the data disagree by about a factor of 10. Since it is difficult to correct the data for desorption processes (both from the evaporator and the chamber) under continuous evaporation

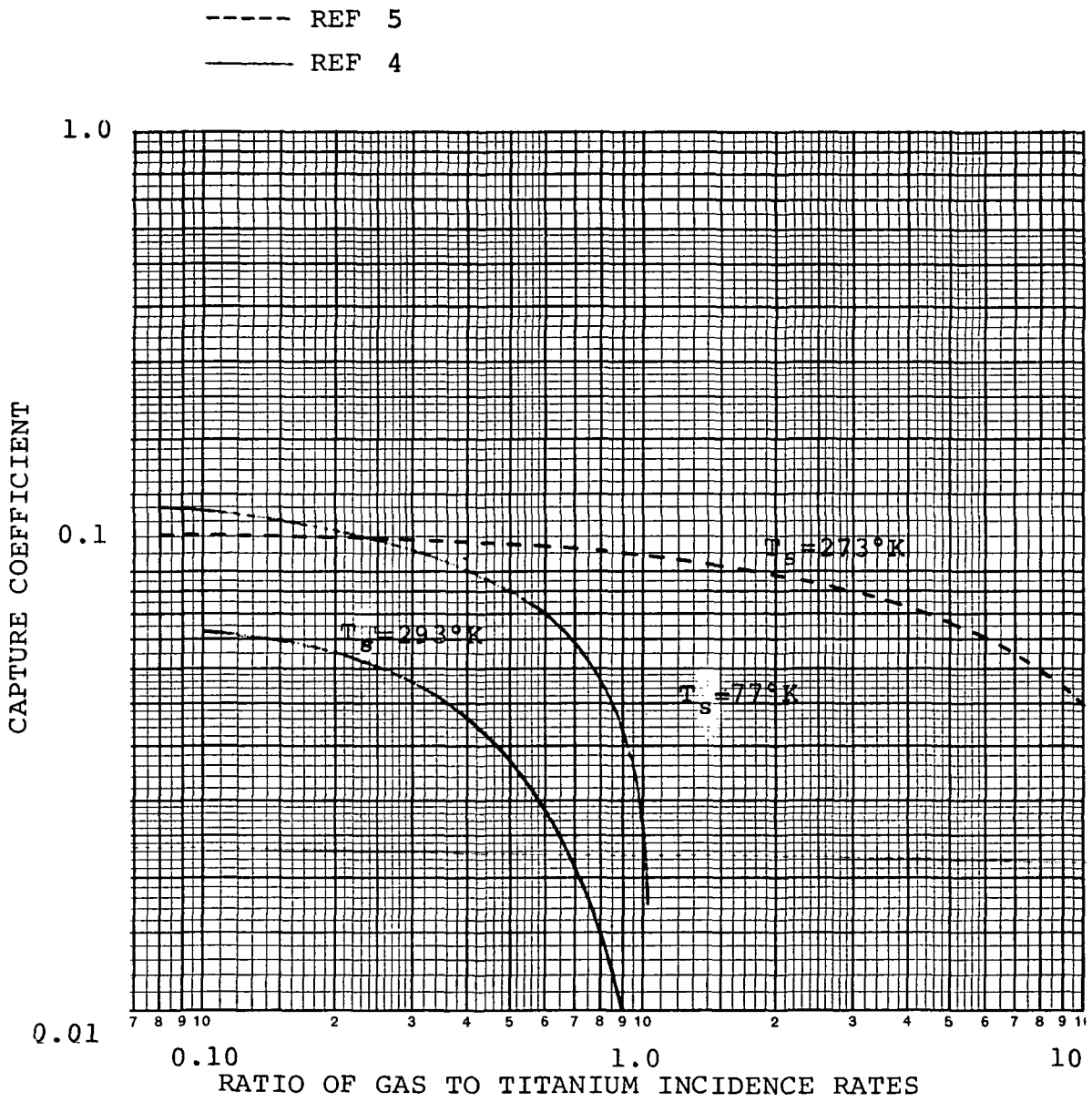

Figure 3

Hydrogen Capture Coefficient as a Function of Substrate Temperature and Incidence Rate for Continuous Evaporation

TABLE I

VARIATION OF H_2 CAPTURE COEFFICIENT

Substrate at Room Temperature		Substrate at ≈ 77°K		
Continuous Evaporation	Batch Evaporation	Continuous Evaporation	Batch Evaporation	Ref.
0.07	0.05	0.14	0.24	4
0.12	----	----	----	5
----	0.011	----	0.23	6
----	0.05	----	0.45	7

conditions, there remains some uncertainty in the value of the capture coefficient. It can be assumed with confidence, however, that the lower limit for the capture coefficient of the diffuse scattered flus is greater than 0.1.

Other points of interest concerning the magntidue of the capture coefficient of batch deposited films are: 1) the value of κ increases with Ti deposition rate 2) κ is significantly higher ($\approx$0.8) when the Ti film is deposited in the presence of a few microns of an inert gas (see ref. 4 and 7). If this increased capture coefficient results from increased background density, then κ will be higher for increased gas incidence rates. 3) the pre-adsorption of certain gases such as N_2 and O_2 have a poisoning effect on κ for H_2 4) κ will undoubtedly be a function of the incident velocity. However, the energy of the beams considered in this study is $<$ 1 eV and since it has been shown that the accommodation coefficient is $\approx$ 1 in this case, it is expected that the effective capture coefficient would not be changed drastically.

Because the size of the sampling probe limits the available pumping area, the appropriate operating conditions for the sorption pumps would be a continuously evaporated Ti film on a 77°K substrate. The evaporators would be placed such that the Ti deposition rate favors those areas where the incident flux is highest (more will be said about this is a later section). Care should be taken to minimize both the heat flux from and the desorption rate of the evaporating surfaces. Based on Moody's data, it will be assumed that the capture coefficient is constant for molecular incidence rates $\leq$ Ti evaporation rates.

4. FLUX DISTRIBUTION AND PUMPING ANALYSIS

Since the exact conditions at the free molecular inlet are not known, general expressions for the flux distribution of the supersonic flow must be developed. Using an equilibrium gas analysis as a basis for comparison, a parametric set of solutions with varying inlet conditions for the spatial distribution of a supersonic inlet sampling system can be derived. From these distributions, conclusions can be drawn concerning the titanium sublimation pumping required to handle the total gas molecular incidence rate as a function of flow parameters in the various stages of the compound inlet, molecular beam forming sampling probe. Provided that the signal-to-noise ratio is high, information on the properties of the gas in the free stream tunnel flow can be derived from measurements of the beam of neutral molecules which pass directly through the sampling probe. Scattering events, either with other molecules or the wall, have two effects; they reduce the signal and combine to produce noise. S/N ratio calculations at the ion source therefore, predict the efficiency of the sampling process as well as the magnitude of the signal presented to the mass spectrometer for composition analysis.

4.1 Equilibrium Gas Analysis

For comparison purposes, analysis of the sublimation pumping of an equilibrium gas at room temperature may be investigated. Consider the following geometry

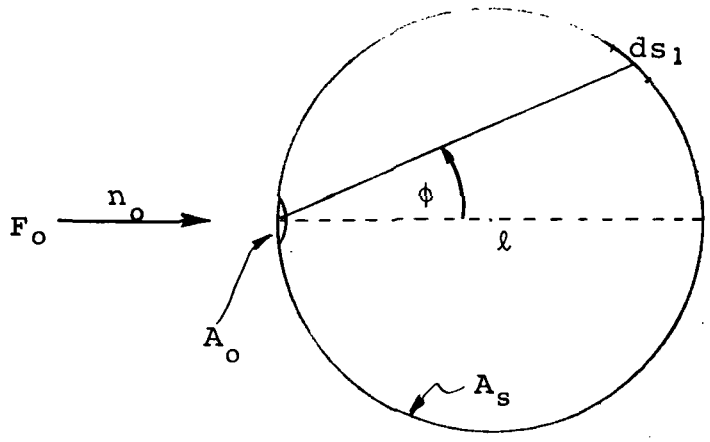

The flux (F_o) entering the spherical volume is

$$F_o = \frac{n_o \bar{v}_o A_o}{4} \text{ molecules/sec} \qquad (4\text{-}1)$$

where

n_o = Free molecular inlet density

$\bar{v}_o$ = Average thermal molecular speed of the gas outside the cavity

A_o = Inlet area.

If A_o is considered a point source, the number of molecules which pass through A_o and collide with unit area (ds_1) in unit time are

$$d\nu_p\ (ds_1) = \frac{A_o\ n_o\ \cos\phi\ d\omega}{v_m^{\,3}\ \pi^{3/2}} \int_0^{\infty} v^3\, e^{-\frac{v^2}{v_m^{\,2}}}\ dv \quad .$$

$$= \frac{A_o\ n_o\ \bar{v}_o}{4\pi}\ \cos\phi\ d\omega$$

$$= \frac{A_o\ n_o\ \bar{v}_o}{4\pi}\ \frac{ds_1}{\ell^2}$$

$$d\nu_p\ (ds_1) = F_o\ \frac{ds_1}{\pi \ell^2} \quad . \tag{4-2}$$

If the capture coefficient of ds_1 is κ_1, then the number of molecules leaving ds_1 per unit time are

$$dF_1' = d\nu_p\ (ds_1)\ [1 - \kappa_1] \quad . \tag{4-3}$$

If it is assumed that the reflected flux (dF_1') is diffuse, then the number of molecules leaving ds_1 and impinging on another element of area (ds_2) per unit time is

$$d\nu_s\ (ds_2) = dF_1'\ \cos\beta\ \frac{d\omega_1}{\pi} \tag{4-4}$$

where β is the angle between the surface normal of ds_1 and $d\omega_1$. This can also be written as

$$d\nu_s\ (ds_2) = d\nu_p\ (ds_1)\ (1 - \kappa_1)\ \frac{ds_2}{\pi \ell^2}$$

$$= F_o\ (1 - \kappa_1)\ \frac{ds_1}{\pi \ell^2}\ \frac{ds_2}{\pi \ell^2} \quad . \qquad (4\text{-}5)$$

However, the diffuse reflected flux incident on ds_2 can come from any surface element of the spherical surface. Thus, the total amount of once reflected flux incident on ds_2 is

$$\nu_s\ (ds_2) = \int_s F_o\ (1 - \kappa_1)\ \frac{ds_1}{\pi \ell^2}\ \frac{ds_2}{\pi \ell^2}$$

or

$$\nu_s\ (ds_2) = F_o\ (1 - \kappa_1)\ \frac{ds_2}{\pi \ell^2} \quad . \qquad (4\text{-}6)$$

If the capture coefficient of ds_2 is κ_2, then the flux leaving ds_2 and incident on ds_3 is

$$d\nu_s\ (ds_3) = \nu_s\ (ds_2)\ (1 - \kappa_2)\ \frac{ds_3}{\pi \ell^2}$$

$$= F_o\ (1 - \kappa_1)\ (1 - \kappa_2)\ \frac{ds_2}{\pi \ell^2}\ \frac{ds_3}{\pi \ell^2} \quad . \qquad (4\text{-}7)$$

The integrated, twice reflected flux incident on ds_3 is

$$\nu_s\ (ds_3) = F_o\ (1 - \kappa_1)\ (1 - \kappa_2)\ \frac{ds_3}{\pi \ell^2}\ . \tag{4-8}$$

However, the total scattered flux incident on ds_3 must also include the singly reflected flux. Therefore, the total scattered flux incident on ds_3 becomes

$$(\nu_s)_T\ (ds_3) = \nu_s\ (ds_2) + \nu_s\ (ds_3)$$

$$= F_o\ (1 - \kappa_1)\ \frac{ds_3}{\pi \ell^2}\ \left\{1 + (1 - \kappa_2)\right\}\ . \tag{4-9}$$

If this reasoning is continued, the total (up to n reflections) scattered flux incident on unit area ds is

$$(\nu_s)_T\ (ds) = F_o\ (1 - \kappa_1)\ \frac{ds}{\pi \ell^2}\ \left\{1 + (1 - \kappa_2) + \right.$$

$$(1 - \kappa_2)\ (1 - \kappa_3) + \text{---} + (1 - \kappa_2)$$

$$\left. \text{----}\ (1 - \kappa_n)\right\}\ . \tag{4-10}$$

If it is assumed that the capture coefficient is independent of the number of surface collisions, $\kappa_1 = \kappa_2 = \text{---} = \kappa_n$ and

$$(\nu_s)_T\ (ds) = F_o \frac{ds}{\pi \ell^2} \left\{ (1 - \kappa) + (1 - \kappa)^2 + \text{-----} + (1 - \kappa)^n \right\} .$$

(4-11)

Besides this multiply reflected flux incident on ds there is also a component of primary flux. Therefore, the total collision frequency on ds is

$$\nu_T\ (ds) = d\nu_p\ (ds) + (\nu_s)_T\ (ds)$$

$$= F_o \frac{ds}{\pi \ell^2} \left[1 + (1 - \kappa) + (1 - \kappa)^2 + \text{----} + (1 - \kappa)^n \right] . \qquad (4\text{-}12)$$

The infinite series converges

$$\sum_{n=o}^{\infty} (1 - \kappa)^n \longrightarrow \frac{1}{\kappa} . \qquad (4\text{-}13)$$

Therefore,

$$\nu_T\ (ds) = F_o \frac{ds}{\pi \ell^2} \frac{1}{\kappa} . \qquad (4\text{-}14)$$

If the total incident flux on the spherical surface (A_s) is desired, $\nu_T\ (ds)$ can be integrated; the result being

$$\nu_T A_s = \frac{F_o}{\kappa} = \frac{\nu_o}{\kappa} A_o \qquad (4\text{-}15)$$

where ν_o is the flux collision frequency per unit area on A_o.

If $A_o << A_s$, the molecular flux leaving the spherical cavity can be neglected and

$$\frac{n_i \bar{v}_i}{4} A_s \kappa = \frac{n_o \bar{v}_o}{4} A_o \qquad (4\text{-}16)$$

where n_i and $\bar{v}_i$ are the molecular density and average velocity inside the cavity. If the temperature of the gas is the same inside and outside,

$$n_i = \frac{n_o A_o}{\kappa A_s} \quad . \qquad (4\text{-}17)$$

As an example, assume that the sphere is 6 inches in diameter with a continuously operating sublimator evaporating titanium onto A_s. Assume also that

$$n_o = 10^{13} \text{ cm}^{-3} \text{ (approximately } 3 \times 10^{-4} \text{ Torr)}$$

$$A_o = 4.9 \times 10^{-4} \text{ cm}^2 \quad (d_o = .025 \text{ cm})$$

$$A_s = 7.3 \times 10^{2} \text{ cm}^2.$$

For $\kappa = 0.1$,

$$n_i = 6.7 \times 10^7 \text{ cm}^{-3} \ (\approx 2 \times 10^{-9} \text{ Torr}).$$

This is equivalent to a pumping speed

$$C\ (n_o - n_i) = S_1\ n_i$$

or

$$S_1 = C\ \frac{n_o}{n_i}\ . \quad (n_i << n_o) \tag{4-18}$$

However,

$$C = \frac{\bar{v}_o}{4}\ A_o \tag{4-19}$$

and

$$S_1 = \frac{\bar{v}_o\ A_o\ n_o}{4\ n_i} = \frac{\bar{v}_i}{4}\ A_s\ \kappa \tag{4-20}$$

which for H_2 at room temperature is

$$S_1 = 3.25 \times 10^3 \text{ liters/sec.}$$

The pumping speed per unit area is therefore

$$\frac{S_1}{A_s} = 4.5 \text{ liters/sec - cm}^2 \tag{4-21}$$

which is about ½ the value reported in the literature (for example see refs. 6 and 8). If it is assumed that each evaporated titanium atom can capture a gas molecule at the surface (A_s), and since $\nu_T \kappa = \nu_o \frac{A_o}{A_s}$, the evaporation rate must be

$$E_{Ti} = \frac{n_o \bar{v}_o A_o}{4 \kappa} \text{ atoms/sec} \qquad (4\text{-}22)$$

$$= 3.9 \times 10^{14} \text{ atoms/sec}$$

or

$$\dot{m}_{Ti} = 3.1 \times 10^{-8} \text{ gm/sec.} \qquad (4\text{-}23)$$

These results assume that both the molecular flux and the evaporated titanium are distributed uniformly over A_s. If κ is high (approaching 1) or the incident primary flux is not uniformly distributed, one must take account of the flux distribution. This is, in fact, the situation for a supersonic stream of molecules entering the cavity and is the case to be considered below.

4.2 Supersonic Flow Analysis

Assume, as before, that the flux is entering a sphere through a small orifice but that now it is a supersonic beam traveling with directed velocity U. The interior of the

sphere is continuously coated with Ti and the value of n_1 for various n_o and U is to be established.

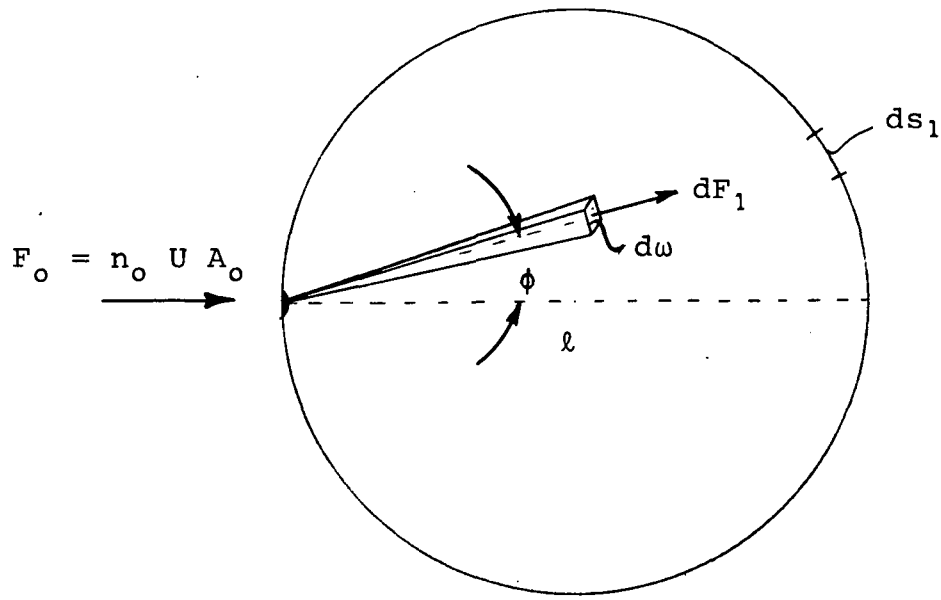

The flux density of molecules traveling at v within dv into solid angle $d\omega$ at an angle ϕ with respect to the axis is

$$\frac{dF_1\ (v,\ \phi)}{A_o} = n_o\ v'^3\ f\ (v)\ dv'\ \cos\phi\ d\omega \qquad (4\text{-}24)$$

where $d\omega = \sin\phi\ d\phi\ d\theta$ and v' is the relative velocity of the molecules with respect to the sampling probe. A_o will again be treated as a point source. Since

$$\vec{v}' \equiv \vec{U} + \vec{v} \text{ and } f(v) \equiv \frac{1}{\pi^{3/2}\ v_m^{\ 3}}\ e^{-\frac{v^2}{v_m^{\ 2}}}\ ;$$

and using the transformation variables

$$\vec{V} = \frac{\vec{v}'}{v_m} \text{ and } \vec{S} = \frac{\vec{U}}{v_m}\ ,$$

the flux density can be expressed as

$$\frac{dF_1\ (\phi)}{A_o} = \frac{n_o\ v_m\ \cos\phi\ d\omega}{\pi^{3/2}} \int_o^{\infty} V^3 \exp - \left[V^2 - 2VS\ \cos\phi + S^2\right] dV. \qquad (4\text{-}25)$$

After the V integration, this becomes

$$\frac{dF_1(\phi)}{A_o} = \frac{n_o v_m \cos\phi \, d\omega}{2\pi^{3/2}} \left\{ e^{-S^2} (1 + S^2\cos^2\phi) + e^{-S^2\sin^2\phi} \right.$$

$$\left. \sqrt{\pi}\, S\cos\phi \left(\frac{3}{2} + S^2\cos^2\phi\right) \left[1 + \text{erf}\,(S\cos\phi)\right] \right\} . \qquad (4\text{-}26)$$

Now assuming $S^2 > 10$ and recalling that $v_m = \frac{\sqrt{\pi}}{2}\bar{v}$, eq. (4-26) can be approximated as

$$\frac{dF_1(\phi)}{A_o} = \frac{n_o \bar{v} \cos\phi \, d\omega}{4\sqrt{\pi}} \left\{ e^{-S^2\sin^2\phi} S\cos\phi \left(\frac{3}{2} + S^2\cos^2\phi\right) \right.$$

$$\left. \left[1 + \text{erf}\,(S\cos\phi)\right] \right\} . \qquad (4\text{-}27)$$

For axial $d\omega \left[d\omega = \frac{ds}{\ell^2}\right]$ this becomes

$$\frac{dF_1(o)}{A_o} = \frac{n_o v_m \, d\omega}{2\pi} \left\{ 2S \left(\frac{3}{2} + S^2\right) \right\}$$

or

$$dF_1(o) = F_o \left[\frac{3}{2} + S^2\right] \frac{ds}{\pi \ell^2} \tag{4-28}$$

For non-zero ϕ, it is clear that the $e^{-S^2 \sin^2\phi}$ term will dominate the flux distribution and therefore, the majority of the flux will be concentrated along the axis. If, as in the equilibrium situation, the collision frequency on an elemental surface area is investigated, some insight into the pumping problem can be gained. The primary flux collision frequency at ds_1 can be expressed as

$$dF_1(\phi) = d\nu_p(ds_1) = n_o A_o U \cos^3\phi \left\{ e^{-S^2 \sin^2\phi} \left[1 + \text{erf}\ (S \cos\phi)\right] \left[\frac{3}{2} + S^2 \cos^2\phi\right] \right\} \frac{ds_1}{2\pi R^2} \quad . \tag{4-29}$$

$$d\nu_p(ds_1) = n_o A_o U \cos\phi \left\{ e^{-S^2 \sin^2\phi} \left[1 + \text{erf}\ (S \cos\phi)\right] \left[\frac{3}{2} + S^2 \cos^2\phi\right] \right\} \frac{ds_1}{2\pi \ell^2} \quad . \tag{4-30}$$

$$d\nu_p(ds_1) = F_o \cos\phi \left\{ \Phi \right\} \frac{ds_1}{2\pi \xi^2} \qquad (4\text{-}31)$$

where

$$\Phi = e^{-S^2\sin^2\phi} \left[1 + \text{erf } (S\cos\phi)\right] \left[\frac{3}{2} + S^2 \cos^2\phi\right] .$$

If it is assumed that the capture coefficient of ds_1 is κ_1, then the flux leaving ds_1 is $dF_1' = d\nu_p (1 - \kappa_1)$. The angular distribution of this scattered flux (dF_1') is in some cases a rather strong function of the molecular incidence angle (ϕ) and the speed ratio (S). However, based on the discussion presented in section 3, together with the fact that the majority of the primary flux (F_1) is incident near the axis and thus, nearly normal to the spherical surface, the assumption will be made that the scattered flux (dF_1') is diffuse. However, since there is some uncertainty concerning the dependence of the capture coefficient on the incident velocity, it will be assumed that κ_1 is less than that for an equilibrium $(S = 0)$ gas but that all other collisions after the first experience of constant capture coefficient equal to that of an $S = 0$ gas. The flux of molecules leaving ds_1 will be

$$dF_1' = d\nu_p (ds_1) \left[1 - \kappa_1\right] . \qquad (4\text{-}32)$$

The fraction of these molecules which are incident on ds_2, having left ds_1 at an angle β with respect to the surface normal to ds_1, is

$$d\nu_s\ (ds_2) = dF_1'\ \cos\beta\ \frac{d\omega_1}{\pi}$$

$$= d\nu_p\ (ds_1)\ (1 - \kappa_1)\ \frac{ds_2}{\pi \ell^2}\ . \qquad (4\text{-}33)$$

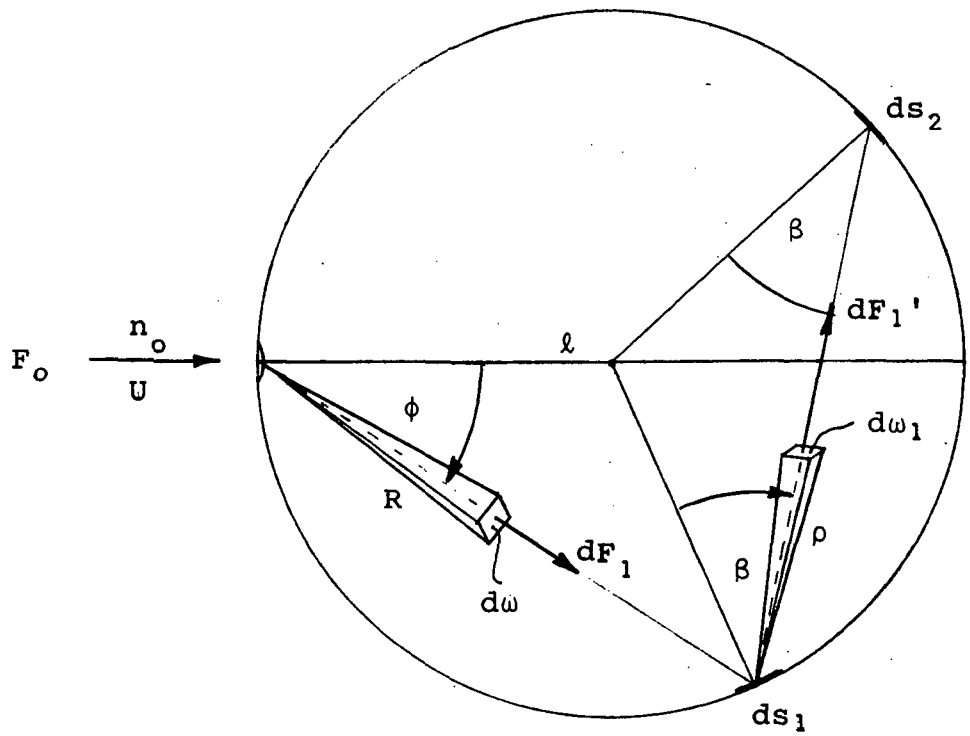

However, once scattered flux incident on ds_2 can come from any ds on the surface and therefore $d\nu_s$ must be integrated over the entire surface. Therefore,

$$\nu_s\ (ds_2) = \int_s d\nu_p\ (ds_1)\ (1 - \kappa_1)\ \frac{ds_2}{\pi \ell^2}$$

$$= \int_s F_o \cos\phi\ \Phi\ (1 - \kappa_1)\ \frac{ds_1}{2\pi\ \ell^2}\ \frac{ds_2}{\pi \ell^2} \qquad (4\text{-}34)$$

or

$$\nu_s\ (ds_2) = \frac{n_o\ U\ A_o}{2\pi}\ (1 - \kappa_1) \int_{\theta=0}^{2\pi} \int_{\phi=0}^{\pi/2} \left\{ e^{-S^2 \sin^2\phi} \right.$$

$$\left. \cos^2\phi\ \sin\phi\ \left[1 + \text{erf}\ (S\ \cos\phi)\right]\ \left(\frac{3}{2} + S^2\cos^2\phi\right) \right\}$$

$$\cos\beta\ \frac{d\omega_1}{\pi}\ d\phi\ d\theta \qquad (4\text{-}35)$$

where ϕ is the polar angle of the primary flux, θ is the azimuthal angle and $d\omega_1 = \sin\beta\, d\beta\, d\eta$. The angle β is the angle between the surface normal of ds_1 and $d\omega_1$, and η is the azimuthal angle of the scattered flux distribution about the surface normal. The assumption of diffuse reflection (or perhaps more correctly described as accommodation and re-emission) allows separation of the polar angles ϕ and β since they are independent variables. This independence of ϕ and β is a result of two effects; one is the assumed diffuse (cosine) distribution and the other is the geometry. The combined effects result in the scattered flux onto unit area, for a given value of ϕ, being a constant and therefore, independent of β (dF_1'/ds_2 is a function of ϕ but independent of β). Therefore, the integrated*, singly reflected flux incident on ds_2 becomes

---

*The integrated results require the use of the assumption, originally made, that $S^2 > 10$. When this assumption is used

$$\int\int \Phi \cos^2\phi \sin\phi \, d\phi \, d\theta = 2\pi \ .$$

$$\nu_s\ (ds_2) = n_o\ U\ A_o\ (1 - \kappa_1)\ \cos\beta\ \frac{d\omega_1}{\pi} \tag{4-36}$$

$$= F_o\ (1 - \kappa_1)\ \frac{ds_2}{\pi \ell^2}\ . \tag{4-37}$$

If the capture coefficient for twice scattered molecules incident on unit area is κ_2, the number of twice scattered molecules leaving ds_2 and incident on ds_3 is

$$d\nu_s\ (ds_3) = \nu_s\ (ds_2)\ (1 - \kappa_2)\ \frac{ds_3}{\pi \ell^2} \tag{4-38}$$

and the integrated, twice scattered flux incident on ds_3 becomes

$$\nu_s\ (ds_3) = F_o\ (1 - \kappa_1)\ (1 - \kappa_2)\ \frac{ds_3}{\pi \ell^2}\ . \tag{4-39}$$

Therefore, the total scattered flux (both once and twice scattered molecules) incident on ds_3 is

$$(\nu_s)_T\ (ds_3) = F_o\ (1 - \kappa_1)\ \frac{ds_3}{\pi \ell^2} + F_o\ (1 - \kappa_1)\ (1 - \kappa_2)\ \frac{ds_3}{\pi \ell^2}$$

$$= F_o\ (1 - \kappa_1)\ \frac{ds_3}{\pi \ell^2}\ \left\{1 + (1 - \kappa_2)\right\}\ . \tag{4-40}$$

If this reasoning is continued for n scattering events, the total scattered collision frequency on unit surface area ds becomes

$$(\nu_s)_T\ (ds) = F_o\ (1 - \kappa_1)\ \frac{ds}{\pi \ell^2} \left\{ 1 + (1 - \kappa_1) + (1 - \kappa_2) \right.$$

$$\left. (1 - \kappa_3) + \text{---} + (1 - \kappa_2)\ (1 - \kappa_3)\ \text{---}\ (1 - \kappa_n) \right\} . \qquad (4\text{-}41)$$

However, it has already been reasoned that $\kappa_1 \neq \kappa_i$ for $2 \leq i \leq n$ but $\kappa_2 = \kappa_3 = \text{----} \kappa_n \equiv \kappa$. Therefore, the total scattered collision frequency becomes

$$(\nu_s)_T\ (ds) = F_o\ (1 - \kappa_1)\ \frac{ds}{\pi \ell^2} \left\{ 1 + (1 - \kappa) + (1 - \kappa)^2 + \right.$$

$$\left. \text{----} + (1 - \kappa)^n \right\} . \qquad (4\text{-}42)$$

The infinite series converges

$$\sum_{n=0}^{\infty} (1 - \kappa)^n \longrightarrow \frac{1}{\kappa} .$$

Besides the scattered flux, there is also incident on ds a component of primary flux. Therefore, the total flux incident on unit surface area ds is

$$\nu_T\ (ds) = d\nu_p\ (ds) + (\nu_s)_T\ (ds) \qquad (4\text{-}43)$$

$$\nu_T\ (ds) = F_o \cos\phi\ \Phi\ \frac{ds}{2\pi\ell^2} + F_o\ \frac{(1 - \kappa_1)}{\kappa}\ \frac{ds}{\pi\ell^2}\ . \qquad (4\text{-}44)$$

Since this total collision frequency is a function of the polar angle ϕ (also through the Φ term), it is advantageous to leave it in differential form. The specific question which needs to be answered is whether the collision frequency on an element ds is greater than can be pumped by continuous Ti evaporation on the same element of surface area. (In the S=0 case, the question did not need to be raised since the collision frequency on ds was constant.) It is therefore, advantageous to solve the problem in differential form (to map out the flux distribution), since the problems will arise for small angles of ϕ off-axis and the sublimators will have to be positioned such that the deposition rates are maximized in these areas. If κ_1 is very small or if the molecular flux is greater than the evaporation rate, then the number density will quickly

equilibrate throughout the volume and, in this case, if n_1 becomes large, gas-gas scattering of the beam will be an important consideration. On the other hand, if κ_1 is of any magnitude at all, a substantial quantity of the total gas can be removed at the first collision (a specific geometry where this is the case will be discussed later).

Knowledge of the integrated flux incident on A_s is also desirable since it gives a comparison with the S=0 case for which experimental data exists. If $\nu_T(ds)$ is integrated over A_s, the total collision frequency becomes

$$\nu_T = F_o + F_o \frac{(1 - \kappa_1)}{\kappa}$$

or

$$\nu_T = n_o U A_o \left\{ 1 + \frac{(1 - \kappa_1)}{\kappa} \right\} . \qquad (4\text{-}45)$$

If it is now assumed that $\kappa_1 < \kappa < 1$ (for example, $\kappa_1 = 0.01$ and $\kappa = 0.1$), the scattered flux is dominant and, because of the complete accommodation of the primary flux, the collision frequency density inside the cavity is assumed to equilibrate to a constant rate over A_s and the conditions closely approximate that of the stationary case. In this instance, as shown in eq. (4-15)

$$\nu_T A_s \approx \frac{\nu_o A_o}{\kappa}$$

or

$$\frac{n_i \bar{v}_i}{4} A_s \kappa \approx n_o U A_o$$

which, for constant temperature, becomes

$$n_i \approx \frac{4 n_o U A_o}{\kappa \bar{v}_i A_s} \approx \frac{2 \sqrt{\pi} n_o S A_o}{\kappa A_s} \quad . \tag{4-46}$$

For a particular example, let

$$n_o = 10^{13} \text{ cm}^{-3}$$

$$U = 1.63 \times 10^5 \text{ cm/sec}$$

$$A_o = 4.9 \times 10^{-4} \text{ cm}^2$$

$$A_s = 7.3 \times 10^2 \text{ cm}^2$$

$$\bar{v} \equiv \left[\frac{8kT}{\pi m}\right]^{\frac{1}{2}} = 3.15 \times 10^4 \text{ cm/sec for } H_2 \text{ at } 300°K$$

$$\kappa = 0.1$$

Therefore,

$$n_i \approx 1.39 \times 10^9 \text{ cm}^{-3} \ (4 \times 10^{-8} \text{ Torr})$$

This is a direct comparison of the supersonic cavity density with the previous equilibrium cavity density, which for the same inlet density and κ yielded $n_i = 6.7 \times 10^7$ cm^{-3}. The above n_i of 1.39×10^9 cm^{-3} corresponds to a surface pumping speed of

$$C\ (n_o - n_i) = S_2\ n_i$$

or, since $n_i << n_o$,

$$S_2 = C\ \frac{n_o}{n_i} \quad . \tag{4-47}$$

However,

$$C = U\ A_o \quad . \tag{4-48}$$

Therefore,

$$S_2 = U\ A_o\ \frac{n_o}{n_i} = \frac{\bar{v}_i}{4}\ A_s\ \kappa \tag{4-49}$$

which is the same conclusion arrived at in the equilibrium calculation. This results from the assumed negligible value of κ_1. The difference in the two cases is that now the cavity density is higher because of the supersonic flux entering through A_o. If the operating criterion of equal pressure

drop across the inlets is imposed, either the inlet density (n_o) has to be lowered, the pumping speed (directly related to κ) has to be increased, or κ_1 has to be increased. The pumping speed is controlled by the average velocity of the dominant flux, at fixed capture coefficient, so either n_o must be decreased or κ_1 increased. Since one of the goals is to maximize n_o, some method must be devised for increasing κ_1. If it is assumed that κ_1 has the maximum value of 1, then from eq. (4-45) it can be seen that the total collision frequency is that of the primary flux (there is no scattered flux for a capture coefficient of 1). However, this concept has little meaning both because the capture coefficient of the surface probably doesn't approach unity (at least for H_2 pumping) and because eq. (4-45) represents the integrated flux into the cavity, which must be uniform if surface pumping speed is to be reasonably interpreted. Therefore, the differential statement of the flux must be used to correctly interpret the results. This was presented as eq. (4-44), namely,

$$\nu_T\ (ds) = F_o\ \Phi\ \cos\phi\ \frac{ds}{2\pi \ell_1^{\,2}} + F_o\ \frac{(1 - \kappa_1)}{\kappa}\ \frac{ds}{\pi \ell_1^{\,2}}\ ^{*} \quad . \qquad (4\text{-}44a)$$

However, in this instance rather than a closed cavity, consider two spherical chambers as shown in Figure 4. This

---

*Subscripts have been used to differentiate the various sampling chambers.

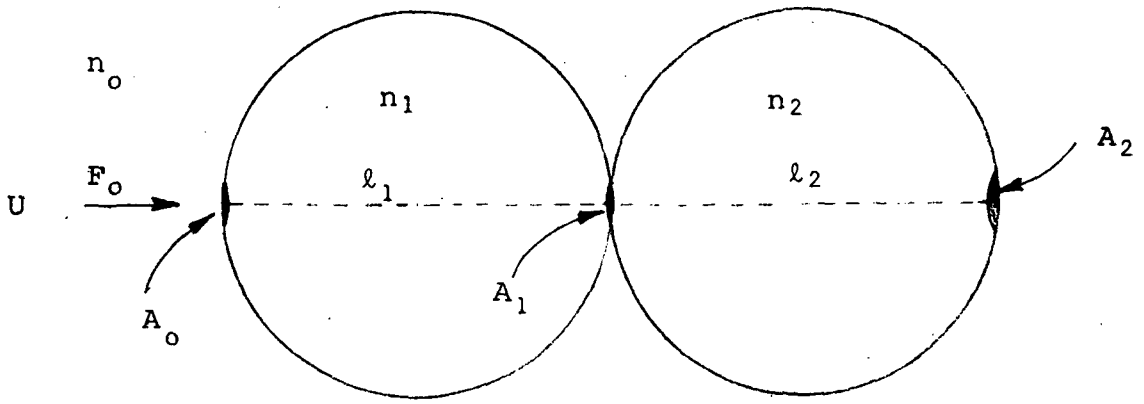

Figure 4
Schematic Representation of a Two-Stage Sampling System

arrangement closely approximates the actual case except that spherical symmetry has been retained rather than the more appropriate conical geometry simply because the scattered flux can be more easily handled analytically with the spherical geometry.

Eq. (4-44a) has been evaluated numerically for various values of the variables and the results are best discussed by considering the two components of the total collision frequency separately; the first term representing the differential primary flux and the second term representing the total (in the sense that it is multiply scattered) scattered flux on unit area.

The angular dependence of the primary flux is presented in Figure 5 in two ways, as $dF_p/d\omega$ vs ϕ and as dF_p/ds vs ϕ so that both the spherical and later the actual geometries can be considered. The two quantities are directly related through the geometry; $dF_p/d\omega$ being independent of the geometrical dimensions and dF_p/ds being related to ℓ_1. The proportionality constant between the two quantities is ℓ_1^2.

$$\frac{dF_p}{d\omega} = \ell_1^2 \frac{dF_p}{ds} \tag{4-50}$$

In these expressions, $d\omega$ is a thin hollow conical shell coaxial with the sampler axis. The scattered flux distribution

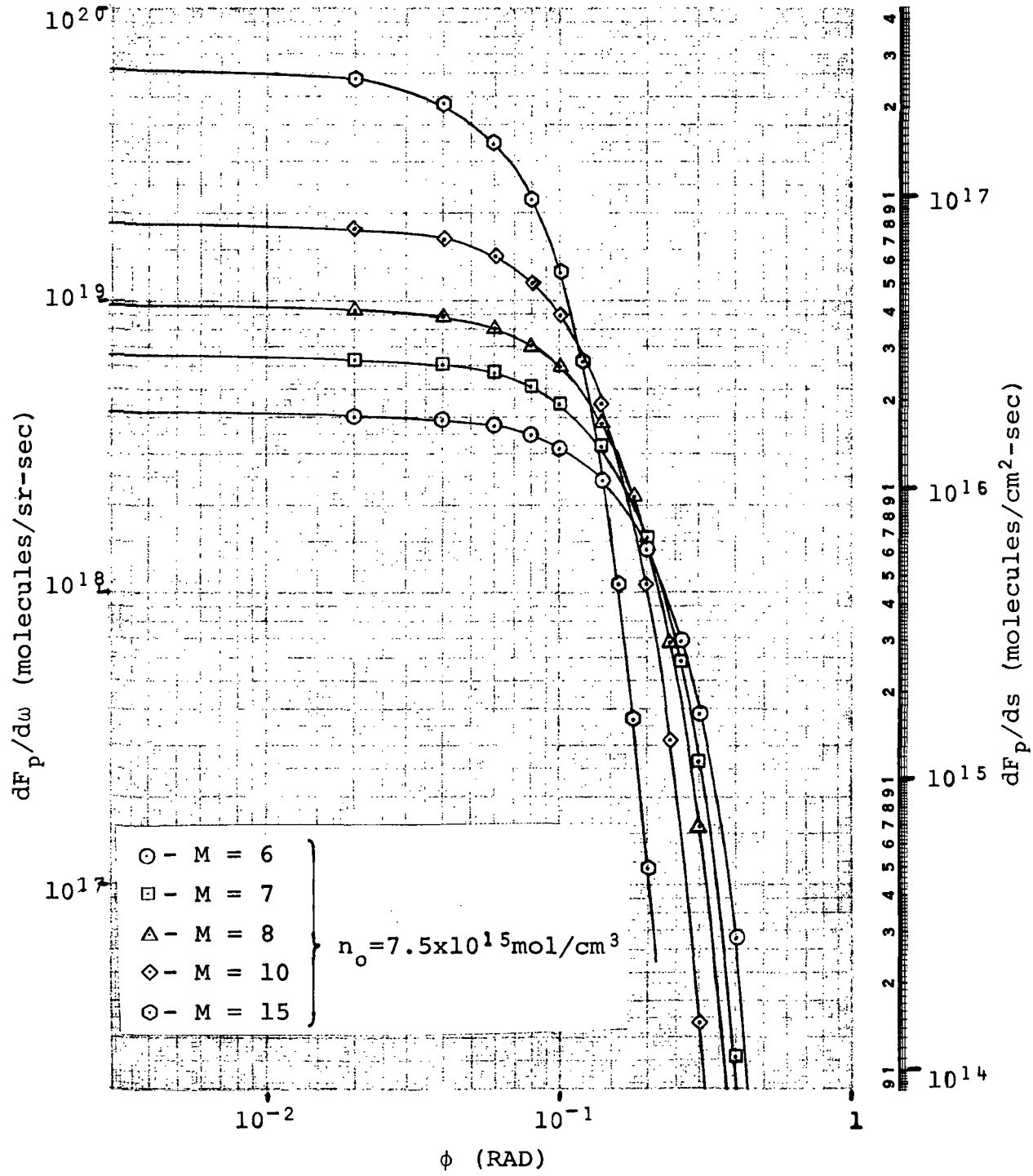

Figure 5

Angular Dependence of the Primary Flux

per unit area is independent of ϕ and $dF_s/d\omega$ is distributed as a cosine function

$$dF_s = F_o \frac{(1 - \kappa_1)}{\kappa} \cos\beta \frac{d\omega_1}{\pi} \quad . \tag{4-51}$$

With expressions for the primary and scattered flux on unit area, three of the important system parameters can be evaluated (1) the effect of gas scattering of the primary flux due to the scattered gas density in the cavity between the inlets, (2) the signal-to-noise ratio (dF_p/dF_s), and (3) the required titanium deposition rate to pump the impinging total flux per unit area.

To calculate the scattered gas density, it must be recalled that the assumption was made that the scattered flux is distributed as a diffuse Maxwellian gas with a temperature characteristic of the surface temperature (T_s). The flux balance at any surface element ds can be expressed as

$$\nu_T' \, (ds) = \nu_T \, (ds) \, [1 - \kappa_n] \tag{4-52}$$

where κ_n is κ_1 if the flux is primary flux and κ_n is κ if the flux is scattered. Since, according to eq. (4-43)

$$\nu_T \, (ds) = d\nu_p \, (ds) + (\nu_s)_T \, (ds),$$

the above expression becomes

$$dF_T' = F_o\ (1 - \kappa_1)\ \Phi\ \cos\phi\ \frac{ds}{2\pi \ell_1^2} + F_o\ \frac{(1 - \kappa_1)}{\kappa}\ \frac{ds}{\pi \ell_1^2}\ . \qquad (4\text{-}53)$$

The second term is unaltered since it represents the total integrated scattered flux after n reflections incident on ds. This total scattered flux is emitted as a cosine distribution from ds with an average velocity ($\bar{v}$) characteristic of the surface temperature. Therefore, the density at any point in the cavity can be expressed as

$$dn\ (\rho,\beta) = \frac{dF_T'\ \cos\beta}{\bar{v}\ dA}\ \frac{d\omega_1}{\pi} \qquad (4\text{-}54)$$

where the geometry is as shown in Figure 6. To investigate the gas scattering attenuation, the integrated density along ℓ_1 must be calculated. The total density at a point is found by integrating eq. (4-54), and can be expressed in integral form as

$$n_T(\ell) = \frac{F_o\ (1 - \kappa_1)}{\bar{v}\ \pi} \left\{ \int_o^{\pi/2} e^{-S^2 \sin^2\phi} \left[1 + \text{erf}\ (S\ \cos\phi)\right] \left(\frac{3}{2} + S^2\ \cos^2\phi\right) \cos^2\phi\ \sin\phi\ \frac{\cos\beta}{\rho^2}\ d\phi \right\} + \frac{F_o\ (1 - \kappa_1)}{\bar{v}\ \pi\ \ell_1^2\ \kappa} \qquad (4\text{-}55)$$

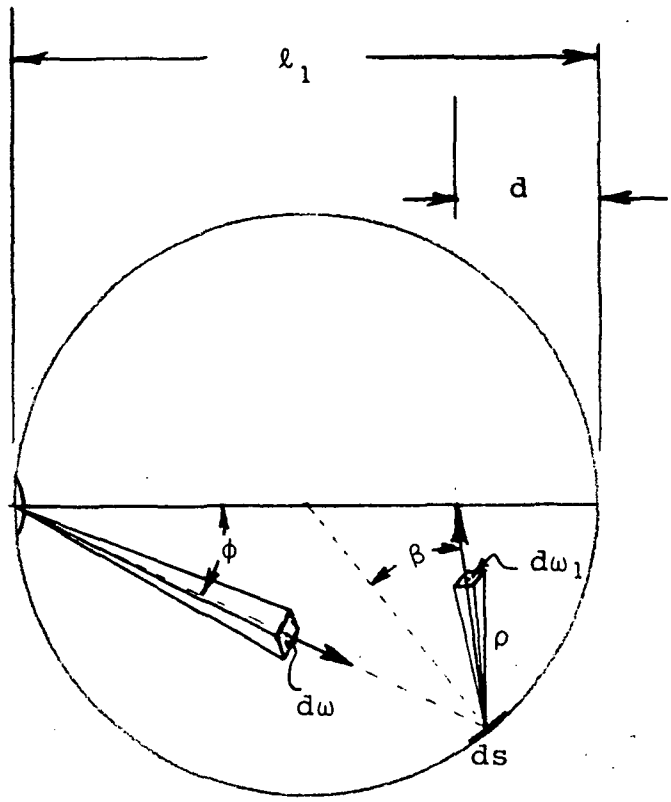

$$d\omega = \frac{ds}{\ell_1^2 \cos\phi} \qquad d\omega_1 = \frac{dA}{\rho^2}$$

$$\rho^2 = d^2 + \ell_1^2 \sin^2\phi - 2\ell_1 d \sin^2\phi$$

$$\frac{\cos\beta}{\rho^2} = \frac{d + \ell_1 \sin^2\phi - 2d \sin^2\phi}{(d^2 + \ell_1^2 \sin^2\phi - 2\ell_1 d \sin^2\phi)^{3/2}}$$

Figure 6
Geometrical Parameters for the Scattered Flux

where β has the functional dependence on ϕ as shown in Figure 6 and the second term is a constant because it has already been integrated in phase space and is therefore, independent of ϕ (it represents a constant density throughout the cavity). The first term is, in general, not integrable and has been solved using computer integration. A typical density profile, based on the first term alone, is shown in Figure 7. The total density profile based on eq. (4-55) is also shown in Figure 7. Exact solutions for the first term of eq. (4-55) were found for $\ell = \ell_1/2$ and $\ell = 0$ $(d = \ell_1)$, in which case $\cos\beta/\rho^2 = 4/\ell_1^2$ and $1/\ell_1^2 \cos\phi$ respectively. The solutions for the integral in these two cases are $4/\ell_1^2$ and $1/\ell_1^2$, assuming that $S^2 >> 1$.

With the shape of the density profile known, it is now possible to establish the gas scattering attenuation of the primary flux in passing through the space between the inlets. The flux which passes a distance ℓ_1 through a gas with a density $n(\ell)$ can be expressed as

$$F = F_o \ e^{-\int_o^{\ell_1} n(\ell)\ \sigma_G d\ell} \qquad (4\text{-}56)$$

where σ_G is the collision cross section for primary flux on scattered gas and the total exponential term is the gas scattering attenuation factor (GSAF). Since the exact

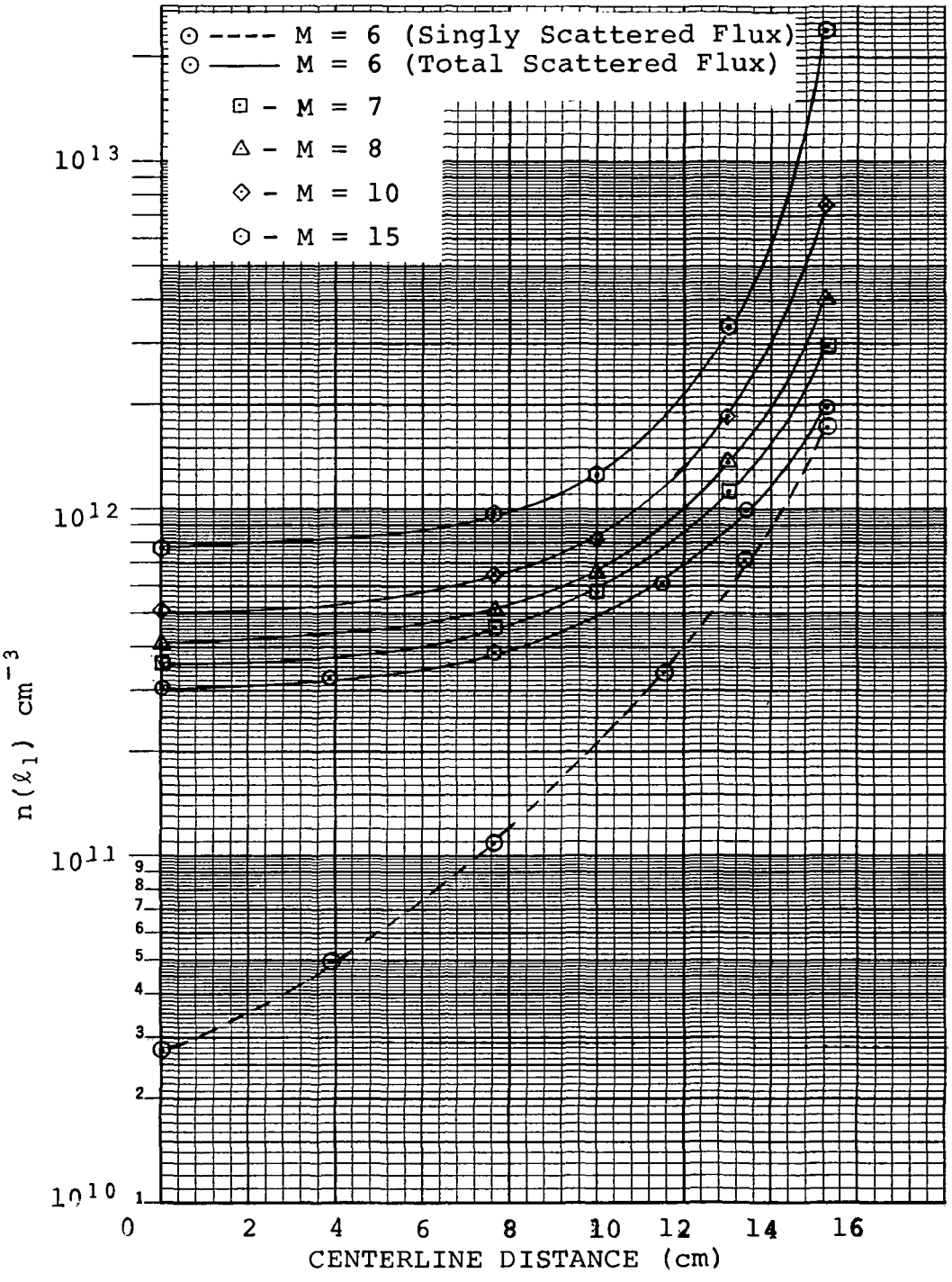

Figure 7

Axial Density as a Function of Distance

functional form of $n(\ell)$ is not known, GSAF was calculated using a numerical approximation for the integral of the density profile and the result for $n_o = 7.5 \times 10^{15}$ cm^{-3}, $\kappa_1 = 0.01$, $\kappa = 0.1$, $\sigma_G = 5 \times 10^{-15}$ cm^2, and $\ell_1 = 15.3$ cm is that GSAF = .955. Since the cavity density profile is a function of the Mach number (speed ratio), the GSAF was determined for various Mach numbers while holding the other parameters constant. These results are shown in Figure 8. Even though the GSAF is approaching a level where it would be of concern, for an increase (of the order of 2 or 3) in any of the constants of the exponential term such as ℓ_1, σ_G or n_o would cause drastic changes in the GSAF especially at the higher Mach numbers, it must be remembered that these calculations represent worst case conditions since the maximum value of n_o was used and pessimistic values for both κ_1 and κ were used. It is not anticipated that gas scattering will be a significant problem.

The signal-to-noise ratio at the mass spectrometer inlet (A_1) can be expressed as

$$\left(\frac{S}{N}\right)_1 = \left(\frac{dF_p}{dF_s}\right) \frac{\bar{v}}{U} \cdot \text{GSAF}$$

$$= \frac{F_o \, \Phi \cos\phi \, \frac{ds}{2\pi \ell_1^2} \, \bar{v} \cdot \text{GSAF}}{F_o \, \frac{(1 - \kappa_1)}{\kappa} \, \frac{ds}{\pi \ell_1^2} \, U} \quad . \qquad (4\text{-}57)$$

$$GSAF = \exp -\sigma_G \int_0^{\ell_1} n(\ell)\, d\ell$$

$$n_o = 7.5 \times 10^{15} \text{ cm}^{-3}$$

$$\kappa_1 = 0.01$$

$$\kappa = 0.1$$

$$\ell_1 = 15.3 \text{ cm}$$

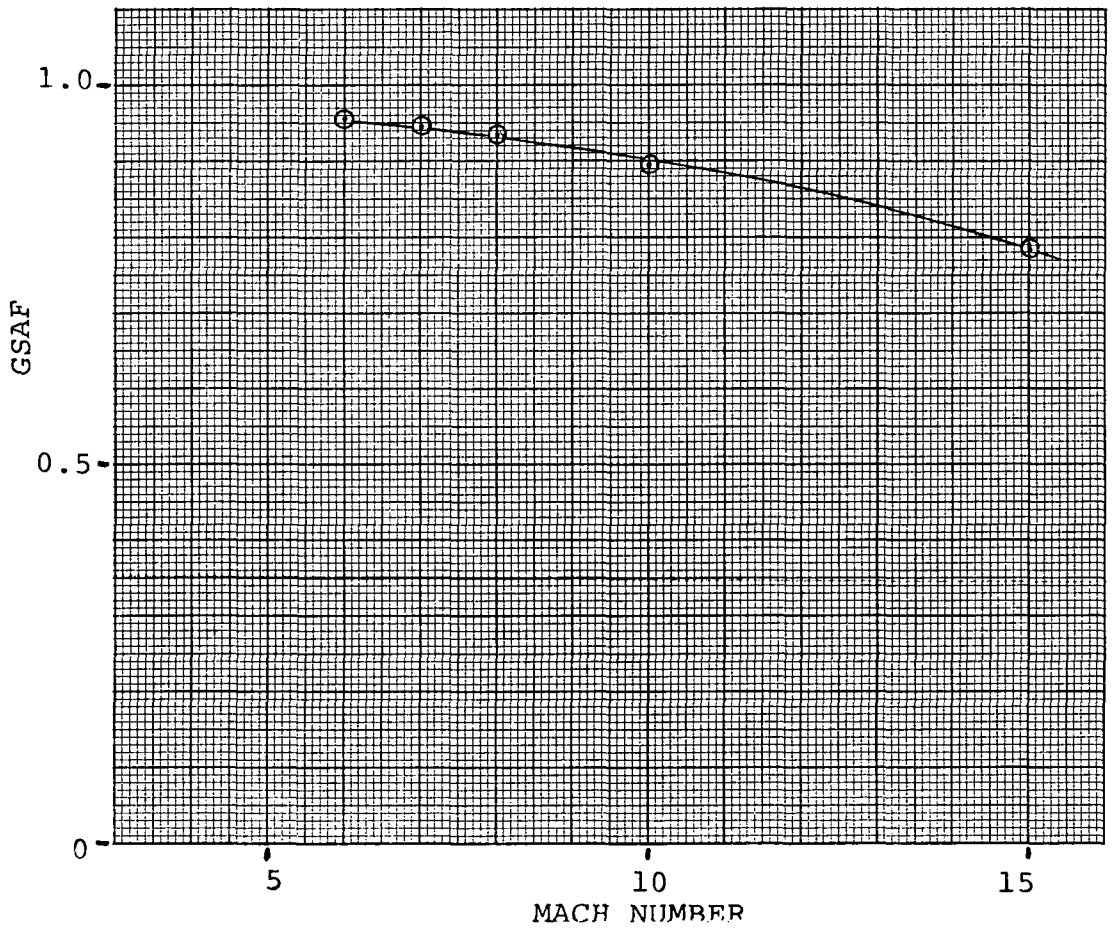

Figure 8

Gas Scattering Attenuation Factor vs. Mach Number

Since the primary flux making up the neutral molecular beam is contained in a small solid angle on the axis, the S/N ratio can be expressed, to a good approximation (see Appendix A), as

$$\left(\frac{S}{N}\right)_1 = \frac{(3 + 2\,S^2)\,\kappa \exp - \sigma_G \int_0^{\ell_1} n(\ell)\,d\ell}{S\,\sqrt{\pi}\,\,(1 - \kappa_1)} \left(\frac{T_s}{T_g}\right)^{\frac{1}{2}}. \qquad (4\text{-}58)$$

For a $M = 6$ flow and the following values for the parameters

$$S = 5.02$$

$$GSAF = .955$$

$$T_s = 77°K$$

$$T_g = 120°K$$

$$\kappa = 0.1$$

$$\kappa_1 = 0.01$$

the S/N ratio is found to be 0.458. This rather low value for the S/N ratio would ordinarily be of concern since an unambiguous interpretation of the signal resulting from the mass spectrometer analyses of the beam of combined primary and scattered flux requires that the S/N ratio be of the order of 50 and at least 10, in which case there is a 10% uncertainty in the composition analysis. There are two

reasons why it is not. First of all,the S/N ratio just calculated represents the value at the mass spectrometer inlet which, as will be shown later, is approximately 1/100th of the value at the ion source some distance ℓ_2 behind the inlet. Secondly, the value of κ_1 and κ were chosen lower than their probable values to evaluate where the real problems would occur. For example, the almost negligible value chosen for κ_1 (0.01) can be substantially increased by a more appropriate arrangement of the geometry; one which is a natural consequence of the anticipated conical geometry. Consider the geometry represented schematically in Figure 9. The separation of the inlets (ℓ_1) is the same as discussed above so that the gas scattering term is not increased. However, in this instance some large fraction of the primary flux (depending on the distribution,which is a function of the inlet conditions) passes through the annular opening which is concentric but not necessarily coplaner with the mass spectrometer inlet. If the region beyond the annular inlet is such that the probability of return of the flux to the inlet plane is small (if it acts as a molecular trap), there results a geometrical enhancement of the S/N ratio, since the effective value of κ_1 is increased. In fact, the annular opening has an effective capture coefficient of unity, if a negligible fraction of the molecules return to the sampling volume. The fact that this annular volume has a large length-to-diameter ratio partly accomplishes this, because each molecule experiences a series of collisions with a

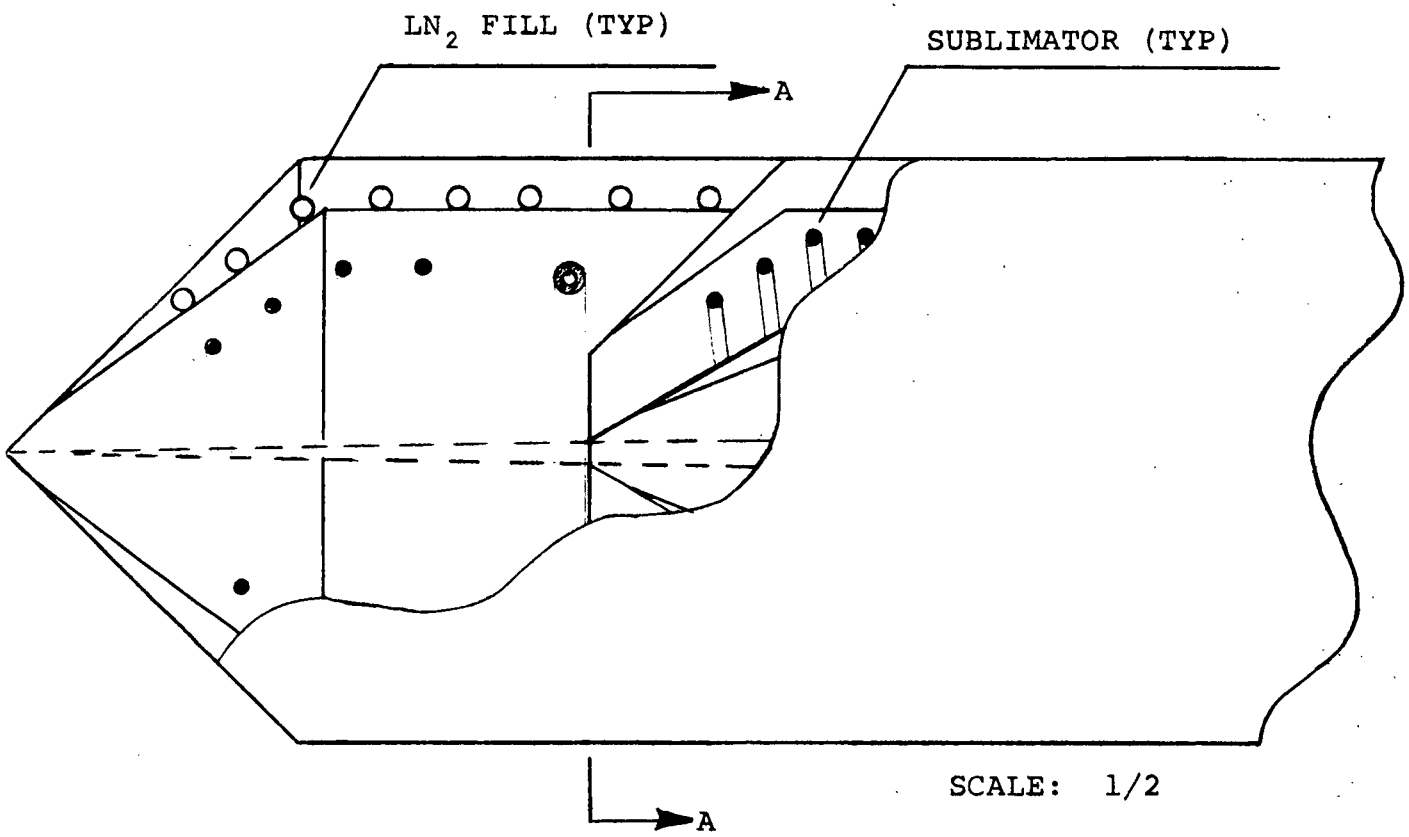

Figure 9
Schematic Representation of Sampling System
(First Two Inlet Stages)

titanium surface before returning to the inlet plane. In addition, if the walls are made up of axial fins rather than flat surfaces, multiple reflections between adjacent fins helps to increase the apparent capture coefficient over that of a flat surface. Although the effect of this type of geometry is difficult to handle analytically, this same type of geometry has been used by JPL (ref. 9) in the design of the molsink and it has been shown by them experimentally that there is about an order of magnitude increase in the effective capture coefficient arising primarily from the geometrical arrangement of the fins such that multiple reflections are caused to occur. A schematic drawing (the section view indicated in Figure 9) of the pumping region containing the finned surfaces is presented in Figure 10.

To improve the S/N ratio, the scattered flux must be reduced since the primary flux per unit solid angle is a function only of the inlet conditions except when gas scattering occurs. Reducing the scattered primary flux has the same effect on the S/N ratio as increasing the capture coefficient (κ_1), since the two are directly related. To evaluate the geometry discussed above, a value for the outer diameter of the annulus was chosen which would allow 50% of the primary flux to pass directly through the sampling chamber (this has the effect of increasing the value of κ_1 to at least 0.5,since the 50% that doesn't hit the wall is removed)

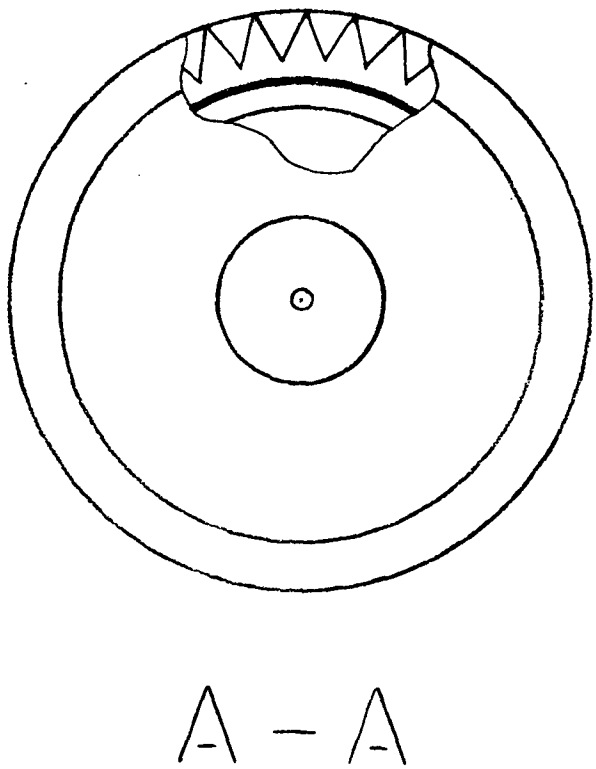

Figure 10
Cross-Sectional View of Finned Pumping Region

and the inner diameter (A_1) was chosen such that the beam diameter at the ion source would be 1.0 cm. With this set of conditions, the S/N ratio at the inlet to the mass spectrometer stage was then evaluated for various values of capture coefficient (κ). These results are shown in Figure 11. Also shown is the dependence of the S/N ratio on Mach number. It can be seen that the S/N ratio in this first free molecular expansion stage is directly related to the capture coefficient (κ) as was indicated in eq. (4-58). It is also seen that although the S/N ratio increases with Mach number the relationship is non-linear because of the effect of the GSAF. The results of these data also show that the S/N ratio is not sufficient to allow an unambiguous determination of the composition of the beam after only one stage in the expansion process. Because of the differences in the angular distribution of the two flux densities (scattered and primary) incident at A_1, a second expansion stage with A_1 as the inlet results in an increase in the S/N ratio and is the analysis to be considered below.

The flux which passes through A_1 is made up of a surface scattered component with a cosine distribution and a primary component. Therefore, the S/N ratio will increase for distances beyond the plane of A_1. However, the total flux entering the second cavity will, after n collisions with the wall, contribute to the noise at a given distance past A_1. It is this S/N ratio which applies to the ion source.

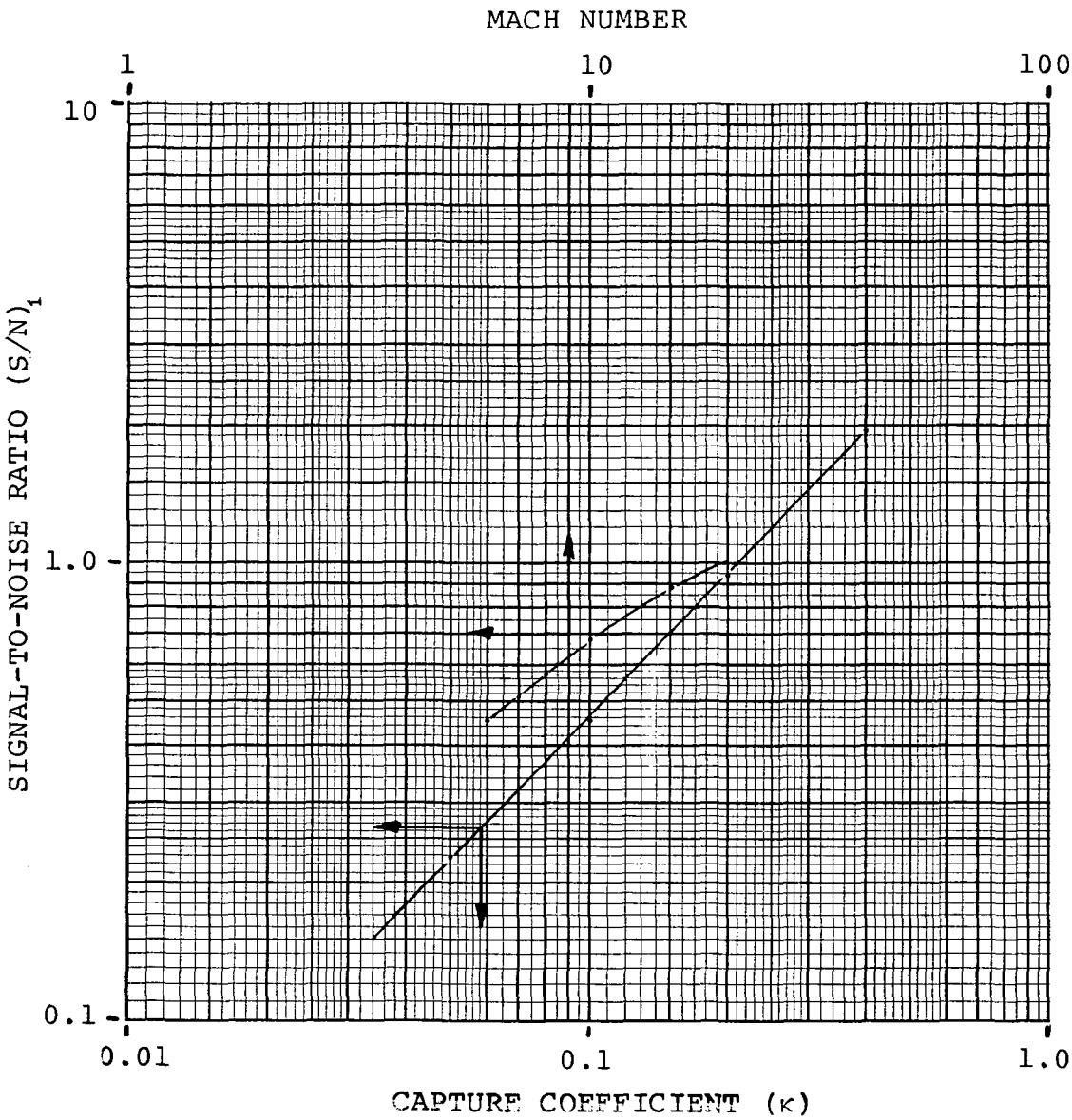

Figure 11

Signal-to-Noise Ratio vs. Mach Number
and Capture Coefficient

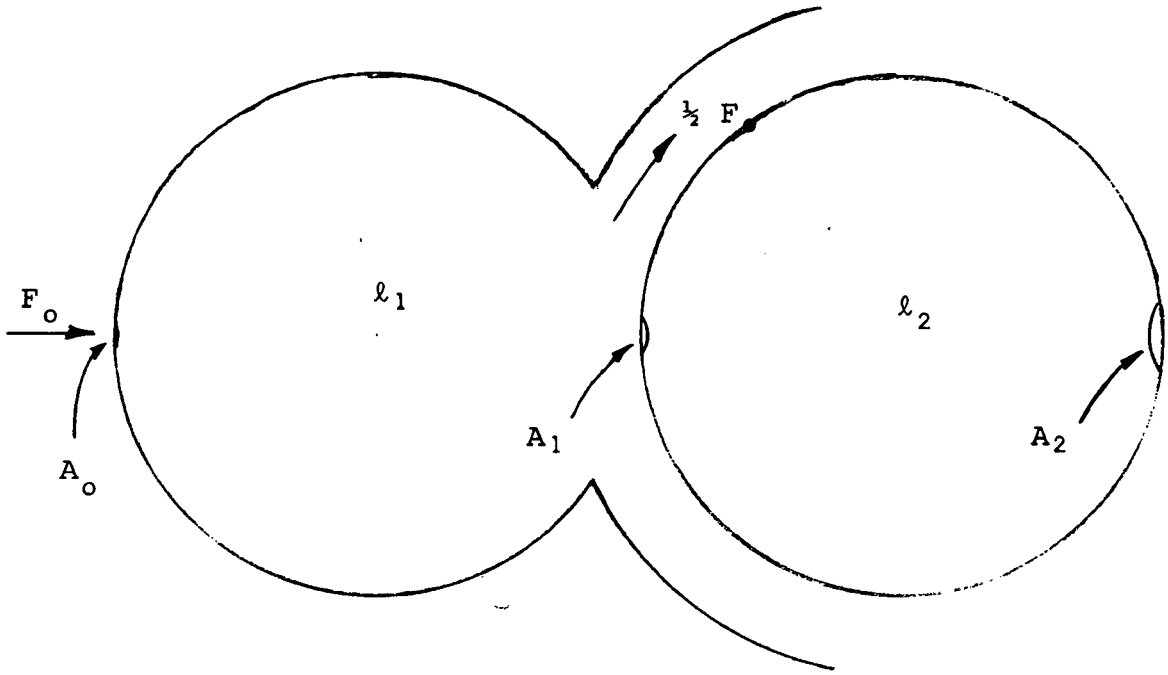

Consider the S/N ratio at A_2, where A_2 might represent the ion source, the inlet to another pumping stage, or the inlet to an ion pump. For the primary flux, the solid angle subtended by A_2 is the same as that of A_1; therefore, the signal will be the same (see Eq. (A-4) of Appendix A)

$$dF_p = \frac{F_o}{\pi} \left[\frac{3}{2} + S^2\right] \frac{A_2}{(\ell_1 + \ell_2)^2}$$

$$= \frac{F_o}{\pi} \left[\frac{3}{2} + S^2\right] \frac{A_1}{\ell_1^2} \quad . \qquad (4\text{-}59)$$

The scattered flux per unit area in the second chamber is a constant and equal to

$$dF_s = \left[F_o \frac{(1 - \kappa_1)}{\kappa} \frac{A_1}{\pi \ell_1^2} \right] \frac{ds}{\pi \ell_2^2} \quad . \tag{4-60}$$

Now letting

$$\left[F_o \frac{(1 - \kappa_1)}{\kappa} \frac{A_1}{\pi \ell_1^2} \right] = F_o' \quad , \tag{4-61}$$

eq. (4-60) becomes

$$dF_s = F_o' \frac{ds}{\pi \ell_2^2} \tag{4-62}$$

which has the same form as eq. (4-2) and represents the conditions for an equilibrium gas at 77°K. Therefore, according to eq. (4-14), the total (n scattering events) scattered flux on A_2 will be

$$\begin{aligned} dF_s &= F_o' \frac{A_2}{\pi \ell_2^2 \kappa} \\ &= F_o \frac{(1 - \kappa_1)}{\kappa^2} \frac{A_1}{\pi \ell_1^2} \frac{A_2}{\pi \ell_2^2} \quad . \end{aligned} \tag{4-63}$$

In this instance, the primary flux passes directly through the cavity without hitting the wall and does not contribute to the scattered flux. The S/N ratio at A_2 is

$$\left(\frac{S}{N}\right) = \frac{\bar{v}}{U} \cdot \frac{dF_p}{dF_s} = \frac{\left(\frac{3}{2} + S^2\right) \kappa^2 \pi \ell_2^2}{(1 - \kappa_1) A_2} \left(\frac{T_s}{T_g}\right)^{\frac{1}{2}} \frac{2}{S \sqrt{\pi}} . \quad (4\text{-}64)$$

This is an improvement of $\frac{\kappa \pi \ell_2^2}{A_2}$ in the S/N ratio at A_1. If $\ell_1 = \ell_2$ and the diameter of A_2 is taken to be 1 cm, this factor is 94. Therefore, the signal-to-noise ratio at the ion source (A_2) is

$$\left(\frac{S}{N}\right) = .458 \ (94)$$

$$= 43 \quad (4\text{-}65)$$

which is large enough to yield meaningful information on the gas composition in the beam even for minor components.

Discussion of the titanium deposition rate required to pump the molecular flux will be delayed until section 6 in which specific sublimation sources are considered.

5. ION SOURCE PARAMETERS

There are two questions remaining concerning the beam flux which passes through A_2:

1. Can this flux be handled by a reasonable pump?
2. Is the beam density at A_2 sufficiently high to be detected (the S/N ratio is now at an acceptable level)?

The beam flux passing through A_2 was shown in eq. (4-59) to be

$$dF_p = F_o \left[\frac{3}{2} + S^2\right] \frac{A_2}{\pi (\ell_1 + \ell_2)^2} \quad . \tag{4-59a}$$

Since $F_o = n_o U A_o$, the beam density at A_2 can be expressed as

$$n_b = \frac{n_o A_o \left[\frac{3}{2} + S^2\right]}{\pi (\ell_1 + \ell_2)^2} \tag{5-1}$$

which, for an $M = 6$ flow, becomes

$$n_b = \frac{7.5 \times 10^{15} \; (6.25 \times 10^{-4}) \left[\frac{3}{2} + 25.2\right]}{4 \; (30.6)^2}$$

$$= 3.33 \times 10^{10} \text{ cm}^{-3} \tag{5-2}$$

which is equivalent to a beam pressure of 4.14×10^{-7} Torr.

If a crossed electron-molecular beam configuration is used as the ion source, the ion current produced in the ionization region for an assumed 0.1 cm wide electron beam operating at an electron beam current density of 5×10^{-3} A/cm^2 would be

$$I^+ = i_e \, n_b \, \sigma \, \lambda \qquad (5\text{-}3)$$

where

$i_e = 5 \times 10^{-3}$ (.1)(1)

$= 5 \times 10^{-4}$ A for a 1 cm dia molecular beam

$n_b = 1.46 \times 10^{10}$ cm^{-3} (equivalent density at 273°K)

$\sigma = 8.8 \times 10^{-17}$ cm^2 for H_2

λ = .785 (Average path length for a 1 cm dia circular beam).

Therefore,

$$I^+ = 5 \times 10^{-4} \, (1.46 \times 10^{10})(8.8 \times 10^{-17})(.785) \text{ A}$$

$$= 5.06 \times 10^{-10} \text{ A}. \qquad (5\text{-}4)$$

If this ion beam is deflected off-axis with an assumed efficiency of 1% and focused into a quadrupole which has an assumed transmission as low as 10%, the ion current at the detector would be 5.06×10^{-13} A. If the gain of the multiplier is 10^5, the output of the spectrometer would be 5.06×10^{-8} A. There is still sufficient dynamic range to detect components in the beam with concentrations 100 times lower than the primary component. In fact, the S/N ratio for components such as O_2 and H_2O will be much higher, since the capture coefficient for these components is higher.

If the primary flux which passes through A_2 is now assumed to stagnate, it is necessary that the density be low enough to be handled by a small pump. The flux passing through A_2 was shown in eq. (4-59) to be

$$dF_p = \frac{F_o}{\pi} \left(\frac{3}{2} + S^2\right) \frac{A_2}{(\ell_1 + \ell_2)^2} \quad .$$

If the cavity walls are at a temperature (T_c) of 273°K, the stagnation density becomes

$$n_S = \frac{4\, n_o\, U\, A_o}{\bar{v}\, \pi\, (\ell_1 + \ell_2)^2} \left(\frac{3}{2} + S^2\right) \tag{5-5}$$

$$= \frac{n_o\, A_o}{\sqrt{\pi}\, (\ell_1 + \ell_2)^2} (3S + 2S^3) \left(\frac{T_g}{T_c}\right)^{\frac{1}{2}}$$

$$= 3.91 \times 10^{11}\ \text{cm}^{-3} \text{ for a } M = 6 \text{ beam.} \tag{5-6}$$

This is equivalent to a pressure of 1.1×10^{-5} Torr. Under stagnation conditions, the flux leaving the cavity is equal to the flux entering and the S/N noise ratio caused by the stagnated flux scattering back into the ion source becomes

$$\frac{S}{N} = \frac{n_b}{n_s} = \frac{3.33 \times 10^{10}}{3.91 \times 10^{11}}$$

$$= 8.5 \times 10^{-2} \quad . \tag{5-7}$$

Since it is desired that the S/N ratio at the ion source be at least 50, the pump in the stagnation cavity must be capable of reducing the stagnation pressure by about a factor of 600 and thus, hold the stagnation cavity pressure at 1.9×10^{-8} Torr. The throughput into (or out of) the cavity is

$$\frac{n_s \bar{v}}{4} A_2 = S P_s \tag{5-8}$$

where P_s is the stagnation cavity pressure required to provide a S/N ratio of 50 at the ion source. Therefore,

$$S = \frac{3.91 \times 10^{11}}{(1.9 \times 10^{-8})\ 16} \left[\frac{8\ (1.38 \times 10^{-16})\ (273)}{\pi\ (1.67 \times 10^{-24})\ (2)}\right]^{\frac{1}{2}} \frac{\pi}{3.54 \times 10^{19}}$$

$$= 1.9 \times 10^{4} \text{ liters/sec.} \tag{5-9}$$

This pumping speed is not realistically achieved with an ion pump. Therefore, the stagnation stage must also have a sublimation pump. Since the beam density at the ion source was shown above to be 3.33×10^{10} cm^{-3}, it is required that the density of the flux returning to the ion source from the stagnation pump be 6.67×10^{8} cm^{-3} to obtain the required S/N ratio of 50. If the same parameters are used as in previous estimates of the sublimation pumping performance, the distance that the supersonic flux travels before striking the wall is the predominant factor controlling the amount of flux which is scattered back into the ion source. The total scattered flux passing back through the ion source from the stagnation pump is related to the beam flux which strikes the wall and can be shown to be

$$\left\{ \frac{F_o}{\pi} (1 - \kappa_1) \left(\frac{3}{2} + S^2\right) \frac{A_3}{\ell^2} + \frac{F_o}{\pi} \frac{(1 - \kappa_1)}{\kappa} \left(\frac{3}{2} + S^2\right) \frac{A_3}{\ell^2} \right\} \frac{A_2}{\pi Z^2} \tag{5-10}$$

where $\ell = \ell_1 + \ell_2 + Z$; Z being the distance that the beam travels in the stagnation pump and A_3 being the area over which the beam is distributed. If this scattered flux entering the ion source is equated to the amount which can be tolerated for the desired S/N ratio, the value for Z can be calculated.

$$\frac{F_o}{\pi}(1-\kappa_1)\left(\frac{3}{2}+S^2\right)\frac{A_3}{\ell^2}+\frac{F_o}{\pi}\left[1+\frac{1}{\kappa}\right]\frac{A_2}{\pi Z^2}=6.67\times10^8\,\bar{v}\,A_2 \tag{5-11}$$

$$Z^2=\frac{n_o\,S\,A_o\left(\frac{3}{2}+S^2\right)\left(1+\frac{1}{\kappa}\right)}{\sqrt{\pi}\,8\,(\ell_1+\ell_2)^2\,(6.67\times10^8)}\cdot\left(\frac{T_g}{T_c}\right)^{\frac{1}{2}} \tag{5-12}$$

where T_c is the temperature of the stagnation pump wall, taken to be 77°K. For an $M = 6$ beam and for $\kappa_1 = 0.01$, $\kappa = 0.1$

$$Z \approx 29 \text{ cm} . \tag{5-13}$$

This value of Z is a result of the low values assigned to κ_1 and κ. If a finned cylindrical pumping surface is used, the effective values of both κ_1 and κ can be increased, thus reducing the value of Z.

6. TITANIUM EVAPORATION SOURCES

Ultimately, the design of the sublimation pumped sampling stages will be chosen on the basis of the maximum molecular flux which can be handled,since it is desirable to operate the sampling probe at the maximum tunnel static pressure possible. One of the basic limitations will be

the maximum titanium deposition rate per unit area which can be achieved. It is therefore, appropriate to investigate the operating characteristics of various sublimation sources with regards to evaporation rate, lifetime and power dissipation. The selected source, producing a given titanium flux density at the cavity walls, can then be compared with the computed gas flux density and the maximum inlet density can be arrived at.

The two most commonly used evaporation sources are the electron beam evaporator, generally referred to as a bulk sublimator since the target is a rod or inget of titanium or in some cases a spool of wire which can be fed into the focal point of the electron gun, and the resistance heated filament evaporator. There are advantages and disadvantages to each type. For example, the bulk sublimator, in general, has a longer life and a higher evaporation rate because the amount of evaporable material is greater and can be run at a higher temperature than the filament source. However, the size and specified orientation do not lead to compatibility with the present requirements. Since the puddle at the focus of the electron beam is molten or nearly so, the source must be located in a downward vertical position to avoid droplet formation from the puddle.

Of the variety of filament evaporators in common use, the two most often used are single wire filaments of either pure titanium or titanium alloys and overwound, stranded

spirals of titanium and some refractory metal on a refractory wire core. There seems to be no distinct reason for selecting a particular filament geometry based on evaporation rate alone. The real basis for selecting a composite or an alloy filament is on the grounds of realiability and repeatability from filament to filament. Since the evaporators are normally operated in the temperature range of 1700 - 2000°K, the titanium readily alloys with the core material of composite filaments and in some cases produces hot spots and subsequent burn out of the filament. Based on the data of Lawson and Woodward (ref. 10) and McCracken and Pashley (ref. 11), the preference for single wire alloy filaments in this application is due primarily to (1) ease of fabrication, (2) reliability and (3) mechanical strength. Presented in Figure 12 are data for the evaporation rate as a function of temperature of both the 85% Ti - 15% Mo alloy wire and pure titanium. It can be seen that there is little difference. For this study, the maximum rate obtainable consistent with a reasonable lifetime is desirable. Shown in Figure 13 are the data of Lawson and Woodward for the effective lifetime of 1.6 mm dia., 85% Ti - 15% Mo wire as a function of temperature. Based on this data and that of Figure 12, one can conclude that the maximum evaporation rate, consistent with a reasonable lifetime (a few hours), would be approximately 7×10^{15} atoms/cm^2-sec. However, based on the data of McCracken and Pashley and information from NRC*, the lifetime of 2.1 mm dia., 85% Ti - 15% Mo wire when operated at a temperature such that the

---

*Private communication of J. C. Maliakal on the performance of the NRC Model 211 Ti getter pump.

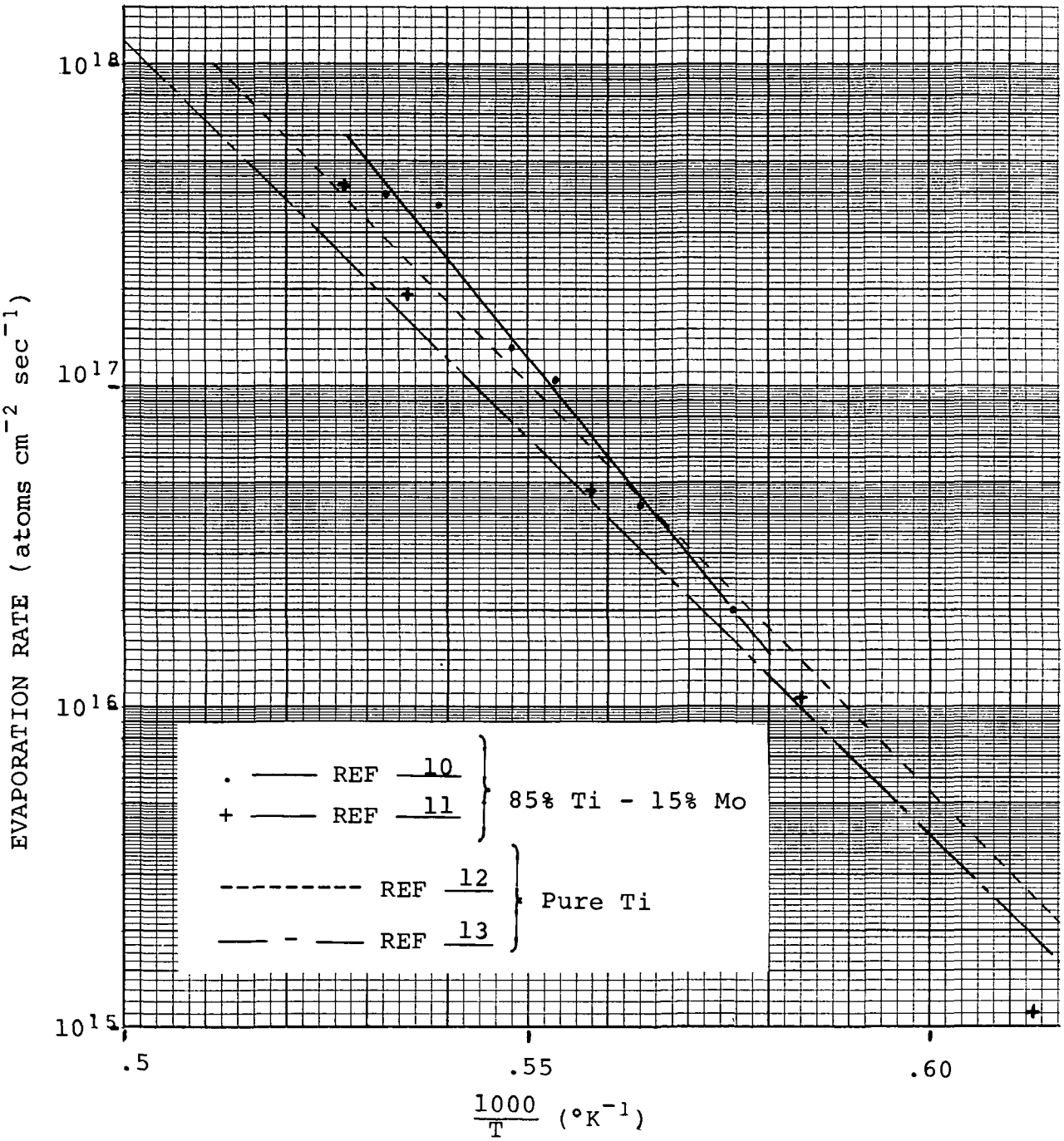

Figure 12

Evaporation Rate of Titanium and Titanium Alloy

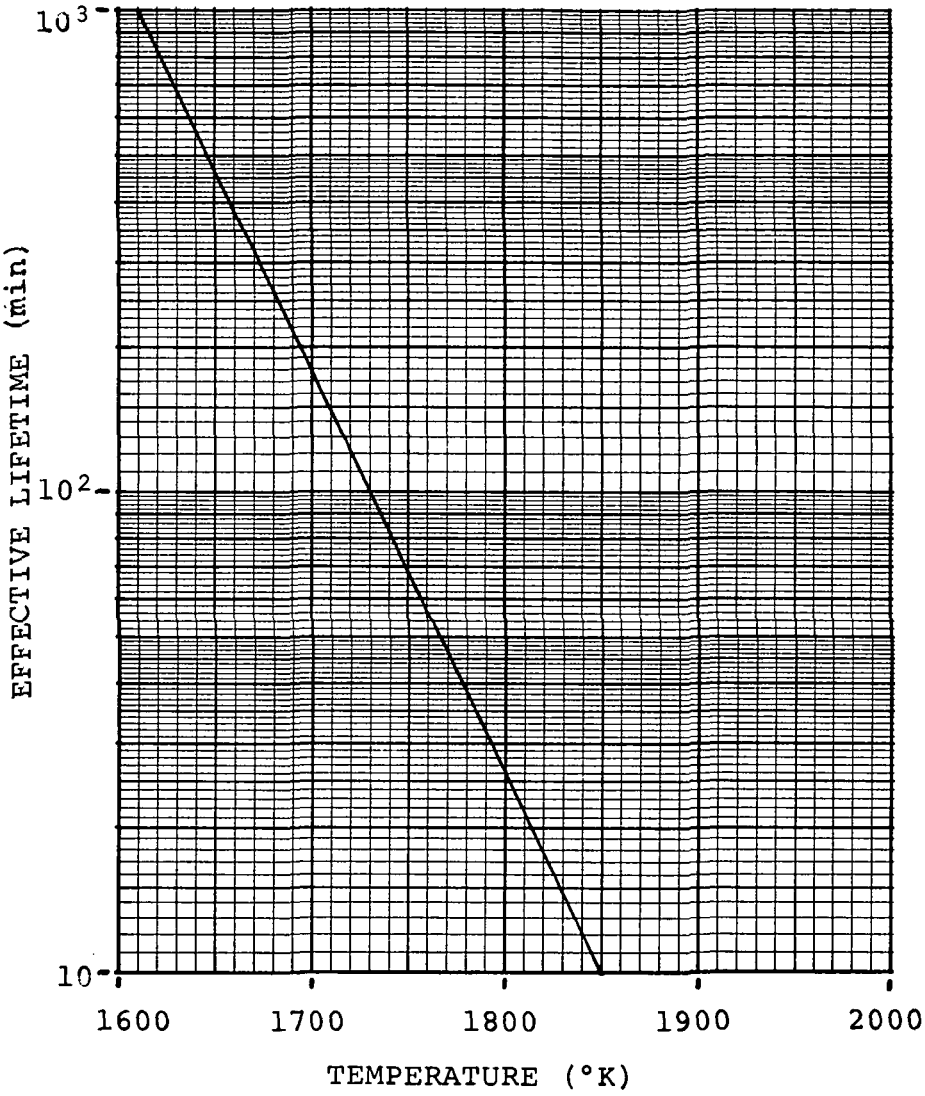

Figure 13

Effective Lifetime vs. Temperature for Titanium Alloy Wire
Ref. 10

evaporation rate is approximately 2×10^{17} atoms/cm^2-sec is around 10 hours. There is apparently some basis for optimization of the maximum evaporation rate with lifetime but for the present it will be assumed that the maximum rate is 2×10^{17} atoms/cm^2 - sec. This rate corresponds to an operating temperature of 1860°K.

The flux density of titanium deposited on the wall of the pumping stage is dependent on the geometry or position of the evaporator with respect to the wall but for the present it will be assumed that the filament is positioned such that a uniform deposit is placed on the wall. In this case, the titanium deposition rate per unit area is equal to the evaporation rate per unit area of filament times the ratio of the filament area to the wall area. Therefore, the deposition rate is approximately

$$\hat{E}_{Ti} = \frac{E_{Ti}}{A_f} \frac{A_f}{A_s} \tag{6-1}$$

$$= \frac{2 \times 10^{17} A_f}{7.3 \times 10^2}$$

$$\frac{\hat{E}_{Ti}}{\ell_f} = 1.81 \times 10^{14} \text{ atoms/cm}^2 \text{ - sec} \tag{6-2}$$

per unit length (in cm) of filament.

It has been postulated earlier that the titanium deposition rate must equal the flux density in order for the pump to operate. Presented in Figure 14 is the data for the total molecular collision frequency as a function of various values of Mach number. It is clear that for these conditions, an unreasonable length of filament is required,especially for the higher Mach number flows. It should be pointed out however, that the tails of the curves (at higher ϕ values), representing the wall collision frequency due to scattered flux, can be pumped in all cases with approximately 100 cm of filament wire. In addition, as pointed out earlier, the values of κ_1 and κ which have been used up to this point are pessimistic values and since the collision frequency is directly related to κ_1 and κ, it is appropriate to choose those values which are considered to be more probable than the ones used for the data in Figure 14. A geometry has already been presented (see Figure 9) for which 50% of the primary flux is trapped; therefore, κ_1 will be set at 0.5. As discussed in Section 3 (see Table I), the minimum value for κ is 0.1 and the maximum value 0.45. Based on this data and recent discussions with representatives of Temescal and Aerovac, it is felt that a value of 0.4 is a more realistic but still a conservative value for κ. These adjustments in κ_1 an κ reduce the scattered collision frequency by a factor of $\approx$ 8. Unfortunately, they have no effect on the primary collision frequency and since the collision frequency at the higher Mach numbers greatly exceeds the deposition rate, the inlet density in these cases must be reduced. At

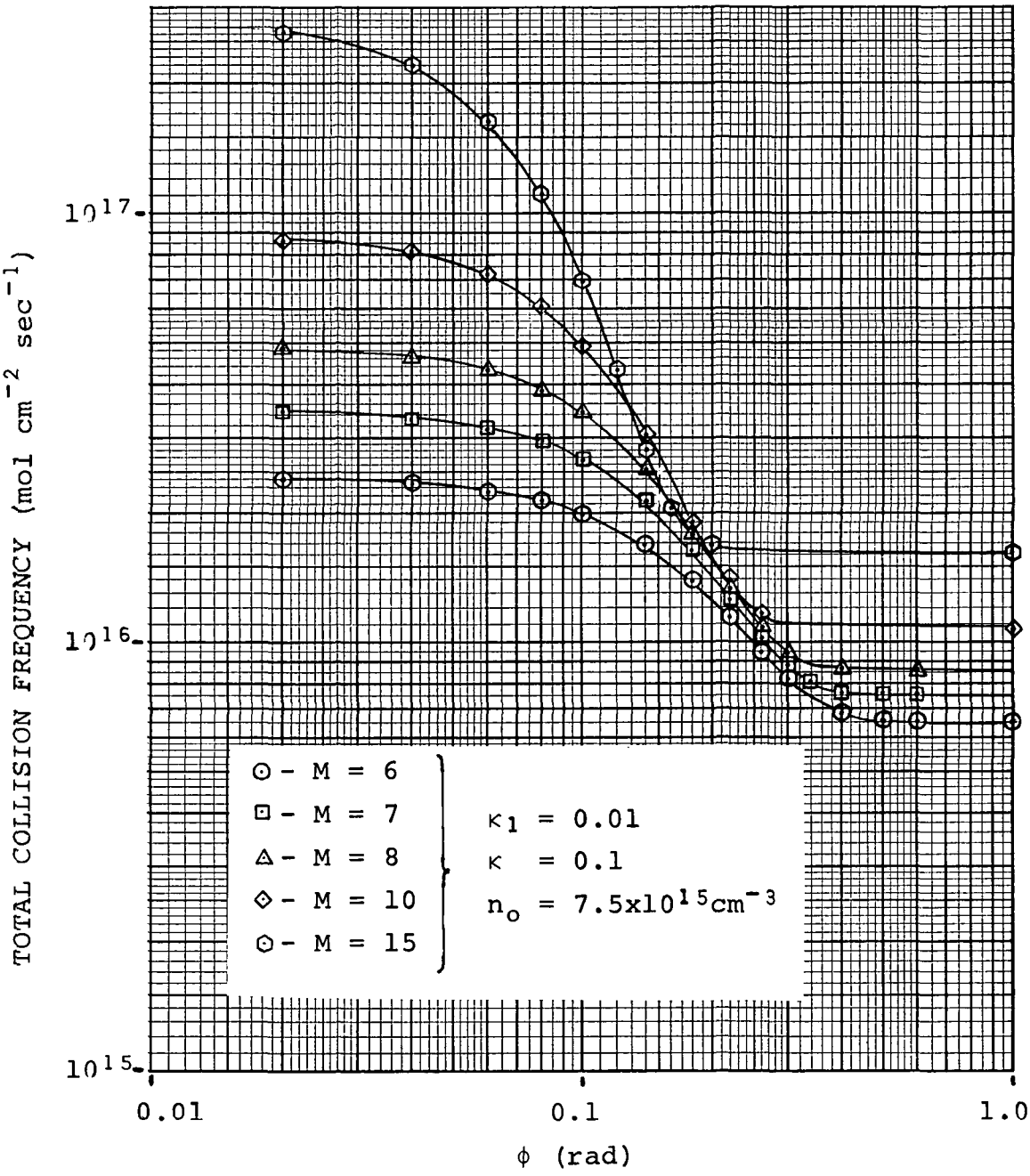

Figure 14

Angular Dependence of the Total Collision Frequency

the lower Mach numbers, the primary flux collision frequency is within a factor of 10 of the value which could be handled and since this flux is distributed over only a fraction of the total pumping surface, the amount which isn't pumped on the first collision will be distributed and added to the scattered flux collision frequency in subsequent bounces. Proper positioning of the evaporators so that the titanium deposition rate is higher on the region where the primary flux hits the wall will help to reduce this problem and since the total evaporation rate is greater than the rate at which molecules enter the sampling volume, it can be assumed that the pump will operate without being overloaded.

A reasonable geometry for the two primary evaporators is as presented in Figure 9. The interstage filament is a .25 inch diameter spiral of 2.1 mm titanium alloy wire formed into a circular evaporator with a mean diameter of 4 inches. For these dimensions, the total length of filament is $\approx$ 100 cm. Therefore, the cavity wall deposition rate in the region where the beam hits the wall is greater than 2×10^{16} atoms/cm^2 - sec, which would be the value for an evaporator positioned such that the deposition rate were uniform. The filament used for the finned, molecular trap region is a simple spiral with a mean diameter of 4 inches and a winding spacing of 3.5 cm. The total filament length is 138 cm, which corresponds to a total evaporation rate of 1.82×10^{19} atoms/sec. The corresponding surface deposition rate is approximately 1.24×10^{16} atoms/cm^2-sec.

Two important topics concerning the operation of the titanium evaporators require comment, namely the desorption or evolution of gas from the filament and the heat load on the cryogenic substrate. The main concerns with respect to the desorbed gas are whether the gas species is capable of being pumped by the titanium substrate and whether the rate adds substantially to the total gas load. The two gas species of concern are hydrogen and methane since the rest are effectively pumped. The question of hydrocarbon gas evolution (especially methane) during the evaporation of titanium in the presence of a predominantly hydrogen atmosphere was experimentally evaluated by Holland (ref 14). The results were interpreted in terms of the carbon and hydrogen impurities in the titanium filaments. It was concluded that there exists a direct relationship between the methane concentration in the vacuum space and the carbon and hydrogen impurities in the titanium. It was further concluded that the effective pumping of hydrogen can only be accomplished with "carbon free" titanium wire; this results from the low capture coefficient of methane. This conclusion is in general accord with the results experienced while operating incandescent surfaces in a vacuum system and has been separately concluded during experiments on orbitron pumped vacuum systems. Since the gas load is a rather strong function of the "history" effects of the wire, it can only be concluded that the successful operation of the pumps requires that the filament wire be as pure as possible and that specific operational procedures be developed, for example a predegassing cycle before a run is a necessity.

An estimate of the power density at the cryosurface, including the energy dissipated by the supersonic gas, the heat load from the filaments and the condensation of the titanium,will indicate whether the heating of the pumping surface is a problem. The region in which the supersonic gas is incident on the pumping surface represents the area where the power dissipation is the highest. The power density from these combined effects can be expressed as

$$\hat{P}_T = \frac{1}{2} m_g U^2 \hat{F} \alpha + \varepsilon \sigma_s \frac{A_f}{A_s} T^4 + \hat{E}_d \left[H_v + \bar{c} \Delta T \right] \qquad (6\text{-}3)$$

where

$\hat{P}_T$ = Total power density

m_g = Molecular mass

$\hat{F}$ = Supersonic flux density

α = Energy accommodation coefficient

ε = Total normal emittance

σ_s = Stefan-Boltzmann constant

A_f = Filament surface area

A_s = Substrate surface area

$\hat{E}_d$ = Titanium deposition rate per unit area

H_v = Heat of vaporization

$\bar{c}$ = Average specific heat.

$$\hat{P}_T = 1.65 \times 10^{-3} + 1.85 + 2.14 \times 10^{-2} \text{ watts/cm}^2$$

The radiant heat is the predominant factor in the total power dissipation. Assuming that the substrate is a liquid nitrogen cooled copper surface with a thickness of approximately .03 inches, the temperature gradient due to a total power dissipation of 1.85 watts/cm^2 would be

$$\Delta T = \frac{\Delta x}{k} \hat{P}_T \qquad (6\text{-}4)$$

where

Δx = Substrate thickness

k = Thermal conductivity

$\hat{P}_T$ = Power density.

$\Delta T = 3.5 \times 10^{-2}$ °K.

Therefore, surface heating is not a problem unless as the titanium deposit builds up its thermal conductivity becomes so low that localized hot spots develop. However, the variation of the capture coefficient with temperature is small and, in addition, it would be unlikely that the effective conductivity would be reduced by two to three orders of magnitude.

7. DISCUSSION OF RESULTS AND CONCLUSIONS

The primary restriction on the use of the sampler under consideration is the maximum molecular flux that may be accepted without scattering which might lead to unacceptable interference in the determination of the free stream molecular composition.

A major requirement in attaining this condition of negligible scattering is the provision for near free molecular flow to occur between the sampler inlet and the mass spectrometer ion source. This requires that the sampler inlet diameter be no larger than the gas mean free path. In addition, to prevent shock formation at the conical skimmer inlet,the inlet lip radius must be as small as possible. However, the fabrication of a conical skimmer with an exterior angle of 45°, a lip radius of 0.025 mm, and a diameter less than 0.25 mm is difficult. Therefore, the molecular density corresponding to a mean free path equal to that inlet dimension is approximately 7.5×10^{15} cm^{-3} and corresponds to an inlet pressure of about 0.1 Torr.

Equally important in maintaining free molecular flow conditions is the requirement that the inlet flux be handled by the pumping capability provided. The considerations in section 6 have shown that with state-of-the-art Ti sublimators, the flux corresponding to the above inlet density can be handled for supersonic flow at Mach numbers up to about ten as long as excessive outgassing of the Ti sublimators does not occur. If the radial dimensions of the sampler

could be increased, the pumping efficiency could be increased; however, in order that the free stream tunnel flow not be excessively disturbed, it is required that the sampler diameter not exceed about 15 cm. Therefore, because of limitations in both fabrication and in pumping of the molecular flux, the maximum inlet pressure that may be handled is 0.1 Torr corresponding to an inlet flux of about 4.8×10^{17} molecules per second for a Mach 6 flow.

Nominal conditions in a hypersonic flow tunnel in which sampling is desired are Mach 6 flow at a static pressure of $\approx$ 50 Torr originating from a stagnation pressure of 7.5×10^{4} Torr and a stagnation temperature of 1940°K. Under these conditions, the free stream temperature for an isentropic expansion of a diatomic gas is 270°K. It may be determined that in order to arrive at the desired density at the sampler inlet, the first (continuum) sampling stage must provide a pressure ratio of at least 250 between the free stream and the sampler inlet, depending on the temperature drop which occurs in the expansion process.

If the expression for axial density given by Ashkenas and Sherman (ref. 15) for a free jet expansion is considered, a pressure ratio of 250 is arrived at about 10 inlet diameters downstream. The inlet conditions in the present case are hypersonic continuum flow as opposed to the inviscid, isentropic free jet expansion considered by Ashkenas and Sherman but the latter's theory should give a rough approximation of the axial expansion process unless viscous effects dominate. For the

free jet expansion, the axial pressure decreases approximately in proportion to the square of the distance so that the pressure drop at an axial distance of 100 hypersonic inlet diameters ($\sim$ 32 cm) would be about 10^4. The assumption has been made here that hypersonic flow without a detached shock can be obtained through a 0.31 cm diameter sharp edged conical inlet. For a free stream pressure of 50 Torr, the inlet pressure would be reduced to about .005 Torr. This is more than an order of magnitude less than the maximum pressure allowable at the sampler inlet. With this large margin for error,due to the assumption of free jet expansion rather than expansion of hypersonic flow,it may be concluded that with adequate pumping available in the hypersonic expansion stage, sufficiently low density flow may be provided at the sampler inlet for successful sampling of the free stream gas composition.

The pumping speed required to fulfill the conditions of a free jet expansion can be estimated from the free stream mass flow rate. The pumping speed so determined may be expressed as

$$S_c = \frac{n_1' \, m_g \, U \, A_1'}{\rho_g} \left(\frac{P_{st}}{P_o}\right) \qquad (7\text{-}1)$$

where

n_1' = Tunnel static molecular density

m_g = Molecular mass

U = Free stream velocity

A_1' = Hypersonic inlet area

P_{st} = Tunnel pitot-static pressure

P_o = Second stage inlet pressure

ρ_g = Gas density.

Assuming that the static temperature is approximately room temperature and that the average molecular weight is 29, the pumping speed for a Mach 6, 1 psia tunnel flow becomes

$$S_c = 2.08 \times 10^5 \, \pi \, \frac{(.125)^2}{4} \quad (6.45) \, \frac{(75) \times 10^{-3}}{4.1 \times 10^{-3}} \quad \frac{\text{liters}}{\text{sec}}$$

$$S_c = 3 \times 10^5 \text{ liters/sec} \qquad (7\text{-}2)$$

This very high pumping speed requirement, therefore, represents a primary limitation. Depending on the pumping speed available for the hypersonic sampling stage, the free stream molecular density will have to be reduced accordingly.

Assuming that the hypersonic flow expansion does occur, the molecular beam density and signal-to-noise ratio were calculated at various points in the inlet-pumping stage expansion process to determine the point in the expansion at which the S/N ratio increased to 50:1. The ion source is situated at that position and the beam density, for the conditions considered, is equivalent to a pressure of 4×10^{-7} Torr. Since the analysis

was performed assuming that hydrogen was the dominant species, the S/N ratio for other constituents of the molecular beam will be higher because the capture coefficient for gases such as N_2, O_2, CO_2 and CO is approximately 0.9. It is estimated therefore, that minor constituents with densities 2 orders of magnitude below the primary beam density can be detected.

The ion beam produced by an electron beam orthogonal to the molecular beam is extracted off axis and focused on the inlet of a quadrupole mass spectrometer. With reasonable assumptions for the extraction efficiency, quadrupole transmission, and multiplier gain; the ion current at the multiplier output was calculated to be approximately 5×10^{-8} A for a primary H_2 beam density of 4×10^{-7} Torr. Therefore, there is sufficient dynamic range to measure the low concentration constituents. To avoid photon noise, it is advisable to use an off-axis multiplier as the quadrupole detector.

The pumping efficiency of continuously operating titanium sublimation sources condensed on a 77°K substrate were analyzed and it is concluded that resistance heated, spiral wound filaments can evaporate titanium at a rate equal to the molecular incidence rate for the maximum inlet density of 7.5×10^{15} cm^{-3} as long as the Mach number is below approximately 10. Under these operating conditions, the lifetime of the filaments is approximately 10 hours. The total power density dissipated at the pumping surface does not appear to pose a problem as long as the thermal conductivity of the con-

densed titanium deposit is within two orders of magnitude of the copper substrate conductivity.

The use of LHe cooled cryosurfaces as pumps for the expansion chambers is limited by two factors (1) the heat input due to the condensation of the molecular flux (estimated to be approximately 14 watts/cm^2) is greater than the maximum to retain pool nucleation boiling (see ref. 16) in the continuum stage but is below the maximum in the other stages (2) the equilibrium vapor pressure of H_2 at 4.2°K is approximately equal to the beam density at the ion source and therefore, results in an unacceptable S/N ratio for the analysis of high H_2 concentration flow. Therefore, for the assumed conditions of this analysis, H_2 being a predominant species, the most probable pumping mechanism is concluded to be either cryogenic sublimation pumping in all the free molecular expansion stages or a combination of LHe cryopumping and cryogenic sublimation pumping; the latter being used at least in the ion source chamber. The possibility of using LH_2 cryosurfaces for the sublimator substrate is an attractive possibility, since the majority of the gases would be cryopumped efficiently (including methane) and the capture coefficient for H_2 should be significantly improved over that at 77°K. The primary limitation is, in the final analysis, concluded to be the pumping speed required in the continuum expansion stage.

APPENDIX A

The expression for the differential primary flux was presented in equation (4-31) as

$$dF_p = F_o \Phi \cos \phi \frac{ds}{2\pi \ell_1^2} \tag{A-1}$$

where

$$\Phi = e^{-S^2 \sin^2 \phi} \left[1 + \text{erf } (S \cos\phi)\right] \left(\frac{3}{2} + S^2 \cos^2 \phi\right)$$

and since $d\omega = ds/\ell^2 \cos\phi$, eq. (A-1) can be re-written as

$$\frac{dF_p}{d\omega} = \frac{F_o}{2\pi} \Phi \cos^2\phi. \tag{A-2}$$

Since dF_p vs ϕ is almost a constant for small values of ϕ (see Fig. 5), the value of $dF_p/d\omega$ evaluated at $\phi = 0$ will be a good approximation for the axial value of dF_p for small $d\omega$. Letting $\phi = 0$ and remembering that $S^2 > 10$ and therefore $\text{erf}(S) \to 1$ reduces eq. (A-2) to

$$\frac{dF_p(o)}{d\omega} = \frac{F_o}{2\pi} (3 + 2S^2) \tag{A-3}$$

APPENDIX B
LIST OF SYMBOLS

A	Nozzle Exit Area (cm^2)
A^*	Nozzle Throat Area (cm^2)
A_o	Free Molecular Inlet Area (cm^2)
A_1	Mass Spectrometer Inlet Area (cm^2)
A_2	Inlet Area to Probe Stagnation Stage (cm^2)
A_3	Distributed Area of the Beam in the Stagnation Pump (cm^2)
A_1'	Hypersonic Inlet Area (cm^2)
A_f	Sublimation Filament Area (cm^2)
A_s	Sublimator Surface Area (cm^2)
$\bar{c}$	Average Specific Heat (cal/gm-°K)
C	Aperture Conductance (liters/sec)
dF_1, dF_p	Differential Element of Primary Flux (molecules/sec)
dF^i	Differential Scattered Flux (molecules/sec)
dF_s	Differential Element of Scattered (n Scattering Events) Flux (molecules/sec)

ds	Elemental Surface Area (cm^2)
$d\omega$	Elemental Solid Angle of Primary Flux (sr)
$d\omega_1$	Elemental Solid Angle of Scattered Flux (sr)
E_i	Beam Incidence Energy (ergs, eV)
$\hat{E}_d$	Titanium Deposition Rate per Unit Area (atoms/cm^2-sec)
E_{Ti}	Titanium Evaporation Rate (atoms/sec)
F_o	Total Flux Entering the Free Molecular Inlet (molecules/sec)
F_o'	$\left[F_o \frac{(1 - \kappa_1)}{\kappa} \frac{A_1}{\pi \ell_1^2}\right]$ (molecules/sec)
F_T	Total Flux Incident on Elemental Area (molecules/sec)
$\hat{F}$	Flux Density (molecules/cm^2-sec)
GSAF	Gas Scattering Attenuation Factor
H_v	Heat of Vaporization (cal/gm)
I^+	Ion Current (amps)
i_e	Electron Current (amps)
k	Thermal Conductivity (cal/sec-cm-°K)

ℓ	Axial Distance (cm)
ℓ_f	Filament Length (cm)
M	Mach Number
m_g	Gas Molecular Mass (gm)
m_s	Solid Molecular Mass (gm)
$\dot{m}_{Ti}$	Titanium Mass Evaporation Rate (gm/sec)
n_o	Free Molecular Inlet or Outside Density (molecules/cm^3)
n_1	Inlet Density at Mass Spectrometer Inlet (molecules/cm^3)
n_2	Background Density at Ion Source (molecules/cm^3)
n_1'	Tunnel Static Molecular Density (molecules/cm^3)
n_b	Molecular Beam Density (molecules/cm^3)
n_i	Interior Cavity Density (molecules/cm^3)
n_s	Probe Stagnation Density (molecules/cm^3)
P_o	Free Molecular Inlet Pressure (psia, Torr)
P_o'	Tunnel Stagnation Pressure (psia, Torr)
P_1'	Tunnel Static Press (psia, Torr)
P_s	Stagnation Cavity Pressure (psia, Torr)
P_{st}	Tunnel Pitot-Static Pressure (psia, Torr)

$\hat{P}_T$	Total Power Density (watts/cm^2)
R	Vector Between the Inlet and Element of Surface Area (cm)
S	U/v_m Speed Ratio
S	Probe Stagnation Pump Speed (liters/sec)
S_1	Sublimator Pumping Speed for an Equilibrium Gas (liters/sec)
S_2	Sublimator Pumping Speed for a Supersonic Gas (liters/sec)
S_c	Pumping Speed at the Continuum Inlet (liters/sec)
(S/N)	Signal-to-Noise Ratio at the Ion Source
$(S/N)_1$	Signal-to-Noise Ratio at Mass Spectrometer Inlet
T_o	Gas Temperature at the Free Molecular Inlet (°K)
T_o'	Tunnel Stagnation Temperature (°K)
T_1'	Tunnel Static Temperature (°K)
T_c	Stagnation Pump Substrate Temperature (°K)
T_g	Gas Temperature (°K)
T_s	Surface Temperature (°K)

U	Directed Gas Velocity (cm/sec)
$\vec{v}$	Molecular Velocity in the Rest Frame (cm/sec)
$\vec{v}'$	Molecular Velocity Relative to the Inlet (cm/sec)
$\bar{v}$	Average Molecular Speed (cm/sec)
$\vec{V}$	$\frac{\vec{v}'}{v_m}$ = Transformation Variable
v_m	Most Probable Molecular Speed (cm/sec)
Z	Stagnation Pump Length (cm)
α	Energy Accommodation Coefficient
β	Polar Angle for Scattered Flux (rad, deg)
ε	Total Normal Emittance
η	Azimuthal Angle of the Scattered Flux Distribution (rad, deg)
θ	Azimuthal Angle of the Primary Flux Distribution (rad, deg)
κ	Capture Coefficient
κ_1	Capture Coefficient on First Collision
λ	Electron Path Length Through the Ion Source (cm)
ν_p	Primary Flux Collision Frequency (molecules/cm^2-sec)

ν_s	Scattered Flux Collision Frequency (molecules/cm^2-sec)
ν_T	Total Collision Frequency (molecules/cm^2-sec)
$(\nu_s)_T$	Total Scattered Flux Collision Frequency (molecules/cm^2-sec)
ρ	Vector Between Two Surface Elements (cm)
ρ_g	Gas Density (gm/cm^3)
σ	Ionization Cross-Section (cm^2)
σ_G	Collision Cross-Section for Primary Flux on Scattered Gas (cm^2)
σ_ε	Stefan-Boltzmann Constant (ergs/cm^2-°K^4-sec)
ϕ	Polar Angle of the Primary Flux (rad, deg)
Φ	$\in^{-S^2\sin^2\phi}\left[1 + \text{erf}\,(S\cos\phi)\right]\left[\frac{3}{2} + S^2\cos^2\phi\right]$
ϕ_i	Angle of Incidence (rad, deg)
ϕ_r	Angle of Reflection (rad, deg)
$\phi_{r_{max}}$	Angle of Reflected Flux Maximum (rad, deg)

REFERENCES

1. R. E. Stickney: Low Energy Molecular Scattering as a Tool for Studying Gas-Solid Interaction Potentials: Comparison of Theory and Experiment, Structures and Chemistry of Solid Surfaces, edited by Gabor A. Somorjai, John Wiley and Sons, 1969).

2. R. F. Brown, H. M. Powell and D. M. Trayer: Studies of the Velocity Distributions of Incident and Reflected Beams; Sixth Rarefied Gas Dynamics Symposium, edited by Leon Trilling and H. Y. Wachman, Academic Press, p. 1187, 1969.

3. R. L. Caldwell, M. R. Bushy and R. F. Brown: Spatial Distributions from 285 to 2500°K Argon Beams Scattered From an Undefined Copper Surface at Temperatures Between 36 and 285°K, AEDC-TR-69-142, Dec. 1969.

4. R. E. Clausing: A Large Scale Getter Pumping Experiment Using Vapor Deposited Titanium Films; Trans. of the Eighth Vacuum Sym. and Second Int'l. Congress, Vol. I, Pergamon Press Inc., p. 345, 1961. See also: Sorption of Gases by Vapor-Deposited Titanium Films; ORNL-3481, Mar. 1964 (available from CFSTI).

5. T. L. Moody: A Technique for Measuring Capture Coefficients and Application to the Measurement of Hydrogen Adsorption by Titanium; AEDC-TR-65-123 (available as AD-628-380) Feb. 1966.

6. L. Elsworth, L. Holland and L. Laurenson: The Sorption of N_2, H_2 and D_2 on Titanium Films at 20°C and -190°C; Vacuum 15, no. 7, 337, 1965.

7. S. M. Kindall: Adsorption of Hydrogen by a Thin Film of Titanium; AEDC-TR-65-113 (available as AD468-316), Aug. 1965.

8. N. E. Boryukova, M. I. Vinogradov, K. D. Danilov and S. S. Shichlovskii: Cooled Titanium Sorption Pump; Instr. and Exp. Tech. (English Trans of Pribory i Tekhnika Eksperimenta) No. 3, p. 610, May-June 1967.

9. J. S. Griffith: Some Tests for Increase in Friction of Mechanisms of the Mariner-Mars 1969 Spacecraft in the JPL Molsink Space Simulator Chamber, JPL TR-32-1446.

10. R. W. Lawson and J. W. Woodward: Properties of Titanium-Molybdenum Alloy Wire as a Source of Titanium for Sublimation Pumps; Vacuum 17, 205, 1967.

11. G. M. McCracken and N. A. Pashley: Titanium Filaments for Sublimation Pumps; J.V.S.T., 3, 96, 1966.

12. J. W. Edwards, H. L. Johnston and W. E. Ditmars: Vapor Pressures of Inorganic Substances. XI. Titanium Between 1587 and 1764°K., and Copper Between 1143 and 1292°K, J. Amer. Chem. Soc., 75, 2467, 1953.

13. S. Dushman: Scientific Foundations of Vacuum Technique edited by J. M. Lafferty, John Wiley and Sons, p. 697, 1962.

14. L. Holland, L. Laurenson and P. G. W. Allen: The Formation of Hydrocarbon Gas by Titanium Getters Containing Carbon and Hydrogen Impurities; Trans. 8th Nat. Vac. Symp., 208, 1961.

15. H. Ashkenas and F. S. Sherman: The Structure and Utilization of Supersonic Free Jets in Low Density Wind Tunnels; Fourth Rarefied Gas Dynamics Symposium, edited by J. H. de Leeuw, Academic Press, 84, 1966.

16. E. G. Brentari and R. V. Smith: Nucleate and Film Pool Boiling Design Correlations for O_2, N_2, H_2, and He, Proceedings of the 1964 Cryogenic Engineering Conference, Plenum Press, 325, 1965.